Spacetime near the Planck scale as an aperiodic tiling

Research Thesis
In Partial Fulfillment of The Requirements for
the Degree of Master of Science in Physics

Tom Shindelman

Submitted to the Senate of the Technion – Israel Institute of Technology, Haifa

Tishrei 5781, September 2020

The Research Thesis Was Done Under The Supervision of
Prof. Eric Akkermans in The Department of Physics

The Generous Financial Help of The Technion
Is Gratefully Acknowledged

Contents

List of Figures

Abstract

We propose a mapping between renormalization group flows and substitution processes for underlying tilings. A substitution process is a way to iteratively construct complicated structures like lattices and fractals. In our work, we use two-letter substitution processes to describe renormalization group flows with 2x2 matrices. We use this mapping to describe a fractal spacetime manifold, which emerges as part of a quantum gravity theory, by a simpler structure - a tiling. The theory we consider in this work is Quantum Einstein Gravity, an effective quantum gravity theory. It has a complicated renormalization group flow, one that is not easily accessible to analytical solution.

In order to obtain the mapping, we begin with a simpler example of a different theory from a remote field in physics: Efimov physics. This theory describes the fractal bound states of scale-free systems, the original being the Efimov effect, a system of 3 spinless quantum particles. In a setup where each pair of these 3 bodies interact via short range, attractive interaction, and their interaction range vanishes simultaneously with the scattering length going to infinity, the system has 3-body bound states which form a geometric series, with universal scaling. This result is surprising, as only 3-body bound states exist whereas 2-body bound states do not exist, for the system. The series of bound states form a self-similar fractal.

Efimov physics and Quantum Einstein Gravity share an important feature. When examining their renormalization group flows, their fractal features correspond to a limit cycle solution appearing in their flow. Such limit cycle solutions are periodic and they have a discrete scale invariance, resulting in self-similar physical quantities. However, Efimov physics has a very simple renormalization group flow, a single quadratic equation, which makes the distinction between its bound states very clear by inspecting its flow. We use the simplicity of the Efimov physics flow in order to construct a mapping between a quadratic renormalization group flow into a tiling, such that the fixed points of the flow map to a periodic tiling, while limit cycles and aperiodic orbits in the flow map to fractal and aperiodic tilings, respectively. We find that these results also hold for Quantum Einstein Gravity and that the phase transition between the different tiling forms is analogous for both theories, hence relating Efimov physics and Quantum Einstein Gravity into the same universality class.

Nomenclature

- β Renormalization group equation
- λ Scaling factor
- D Hausdorff dimension
- L Length or radius
- m Mass
- m_S Mass of Sierpinski triangle
- $\mathbb{N}$ Natural numbers
- A_i Alphabet
- σ Substitution operator
- k Substitution step or momentum scale
- n_i Number of type i letters in substitution rule
- M Occurrence matrix
- l_0^i Length of type i tile
- l_n^i Total length of type i letters at substitution step n
- ρ_i Density of type i letters
- $\overline{a}$ Average lattice
- $m_i\,(n)$ Number of type i letters at substitution step n
- λ_i Occurrence matrix eigenvalues
- $x\,(n)$ Tiling length at substitution step n
- $u\,(n)$ Fluctuation of tiling length from average lattice
- V_i Potential strength of type i
- $W_i\,(n)$ Work of particle on i sub-tile at substitution step n
- $\hbar$ Reduced Planck constant
- E Energy
- ∇^2 Laplace operator
- l Angular momentum quantum number
- d Dimension
- ζ Interaction strength

- ψ Wave-function
- μ reduced mass
- ξ Dimensionless interaction strength
- χ Radial wavefunction
- θ Polar angle
- ϕ Azimuthal angle
- ξ_c Critical dimensionless interaction strength
- g Boundary condition coupling constant
- L_0 Boundary condition radius
- φ Phase
- $g_\pm$ Fixed points of renormalization group flow of g
- g_k Discrete boundary condition coupling constant or dimensionless gravitational constant
- g^* Fixed point of boundary condition coupling constant g or dimensionless gravitational constant g_k
- $\mathbb{Z}$ Integers
- $\mathbb{C}$ Complex numbers
- Tr Trace over all indices with spacetime integration
- $\mathcal{L}_v$ Lie derivative w.r.t vector field v
- $\overline{g}_{\mu\nu}$ Background metric
- $h_{\mu\nu}$ Dynamical metric
- $\gamma_{\mu\nu}$ Full metric
- $g_{\mu\nu}$ Full metric expectation value
- C Ghost field
- D^2 Covariant Laplace operator
- R_k Scale dependent cutoff
- S_k Scale dependent action
- W_k Scale dependent generating functional
- Γ_k Average effective action
- $\Gamma_k^{(2)}$ Scale dependent exact propagator
- Γ_k^{quad} Quadratic part of average effective action

- R Ricci curvature
- $\mathcal{G}^{(n)}$ Correlation function of n fields
- T Limit cycle period
- Z_{N_k} Graviton field strength renormalization
- $\overline{G}$ Newton's constant
- G_k Scale dependent Newton's constant
- $\overline{\Lambda}_k$ Scale dependent cosmological constant
- η Anomalous graviton dimension
- Λ_k Dimensionless scale dependent cosmological constant
- $u_i\,(k)$ Coupling constant i at scale k
- Λ^* Cosmological constant fixed point

1 Introduction

The structure of our spacetime near and below the Planck scale remains a fascinating and elusive open question in physics to this day. The issue of non-renormalizability of gravity has plagued efforts of formulating a quantum gravity theory for as long as quantum field theory and general relativity exist. Reuter's Quantum Einstein Gravity (QEG), a candidate quantum gravity theory, overcame this barrier by using exact functional renormalization group (RG) [1] to extract a scale-dependent metric. Reuter et al discovered that QEG predicts the emergence of a remarkable fractal spacetime structure, with a scale dependent dimension that approaches 2 near the Planck scale [2]. This conclusion agreed with earlier numerical results of Ambjørn and Loll's theory of causal-dynamical-triangulation (CDT) [3], as well as other quantum gravity theories [4, 5]. Both QEG and CDT attribute fractal properties of the metric to the scale dependent universe they describe. On the other hand, it has been speculated by Litim et al that the dimensional reduction in QEG is related to limit cycles in its RG flow [6]. As their name suggests, limit cycles are cyclic solutions with a discrete period, that occur when the fixed points of the flow become complex. They are found in a variety of self-similar phenomena, e.g. in quantum theories [7–9] and in biology [10, 11], since their discrete scaling symmetry translates to fractal observables. In this work we highlight the relation of the fractal spacetime of QEG to its limit cycles by geometrically representing its RG flow. We find that under a specific mapping [12] limit cycles present as fractal tilings.

In order to achieve this purpose we begin with a discussion of a different fractal phenomenon that is also related to limit cycles and known as "Efimov physics". It is a well studied and thoroughly understood field, the use of which proves useful to us as we formulate a simple probe of the RG flows exhibiting limit cycles.

One of the most remarkable appearances of discrete scale invariance (DSI) in quantum mechanics was the Efimov effect [13], discovered by and named after Efimov in 1970. Efimov discovered that when three spinless particles had vanishing interaction range and infinite scattering length, a set of shallow, fractal three-body bound states with a *universal* discrete scaling factor emerges. The effective description is essentially that of a quantum, massive, neutral particle in an attractive $1/r^2$ potential. Since its discovery Efimov physics proved to be ubiquitous, e.g. the case of a Dirac charged, massless fermions in a Coulomb

potential or in line depinning theory [14, 15]. Physical manifestations of the effect are versatile, including e.g. Feshbach resonance and ultra-cold atoms [16–19]. The RG perspective of these effective theories has been studied extensively in e.g. [9, 20, 21]. It has been shown that the Efimov spectrum is recovered when their flows exhibit limit cycles [8, 22, 23]. In the following, we map Efimov physics to a tiling and then use the insight gained from studying the mapping on its simple, analytic RG flow as a guide for the more complicated QEG case. To better understand the relation of the limit cycles in QEG to its fractal spacetime, we first establish the relation of the Efimov limit cycles and fractal energy levels. To that purpose, we analyze a mapping of the RG flow of Efimov physics to tilings generated by a dynamical substitution process.

Substitution processes had been proven to be great at capturing the properties of aperiodic and DSI physical structures, e.g. quasi-periodic and fractal lattices [24, 25]. The basic quantity representing their dynamics is the occurrence matrix, which sets the rules and determines the spatial evolution of a tiling. We use the substitutions formalism to obtain from a RG flow an occurrence matrix, endowed with the parameters of the Efimov limit cycle. We then test this mapping on QEG and in both cases find that the fractal properties of limit cycles translate into aperiodic and fractal tilings.

2 From Efimov bound states to fractal tilings

2.1 Substitution processes

2.1.1 Fractals and self-similar functions

To understand fractals and self-similarity, a brief introduction to scale invariance is required. We define a scale-invariant function,

$$f(ax) = b(a) f(x). \tag{2.1}$$

Two kinds of scaling symmetries arise from this definition. The first is continuous-scale-invariance (CSI): If a function satisfies the scaling symmetry (2.1) $\forall a$ and corresponding $b(a)$, this scaling relation expresses the continuous self-similarity of the function f. In particular, we have

$$f(ax) = a^D f(x), \tag{2.2}$$

where D is the Hausdorff dimension defined as

$$D = \frac{\ln b}{\ln a}. \tag{2.3}$$

Since the scaling of f is independent of x, its solution is a homogeneous function,

$$f(x) = Cx^D. \tag{2.4}$$

A simple example of continuous scale invariance is the scaling of the mass of a string. If at length L the string has mass m, it is obvious that at length $2L$ the mass of the string will become $2m$. The function describing the relationship between the mass of the string and its length satisfies

$$m(2L) = 2m(L).$$

If we were to choose any scaling for the length of the string, the mass would always be multiplied by that same amount. It follows that a string mass is CSI, namely

$$m(\lambda L) = \lambda m(L), \forall \lambda. \tag{2.5}$$

While the scaling (2.1) is true for CSI functions for any $a, b\,(a)$, discrete-scale-invariant (DSI) functions only satisfy this condition for a pair of *fixed* numbers a, b. In physics, DSI functions most commonly describe self-similar fractals [26], e.g. the Sierpinski triangle, whose scaling symmetry only holds for $a = 2, b = 3$. These numbers describe how to obtain another Sierpinski triangle from the original: halve the side of the original triangle $n \in \mathbb{N}$ times. If one assigns "mass" to the lines within the Sierpinski triangle, the "mass" of the resulting triangle would then be $1/3^n$ of its original value, as shown in figure 2.1. It is important to recognize that this property is unique to the set $\{2, 3\}$ and is not satisfied for any other pair of numbers, namely for the mass of the Sierpinski triangle we have

$$m_{\mathrm{S}}\left(2^N \ell_{\mathrm{side}}\right) = 3^N m_{\mathrm{S}}\left(\ell_{\mathrm{side}}\right), \forall N \in \mathbb{Z}. \tag{2.6}$$

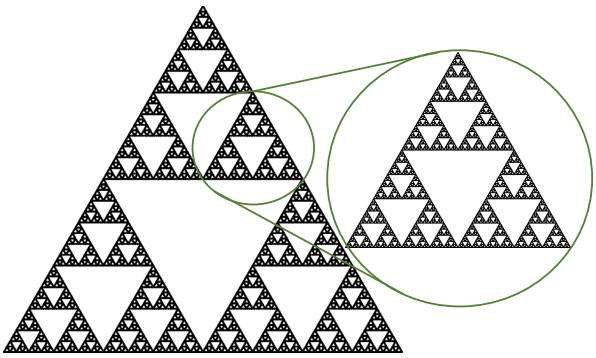

Figure 2.1: The Sierpinski triangle is a self-similar fractal. When cutting the side into quarters ($N = -2$), the mass reduces to $3^N = 1/9$ of its original value.

The discrete scaling relation fractals adhere to expresses that a self-similar fractal contains infinitely many copies of itself, each accessed by correctly rescaling the original object. The DSI properties associated with fractals are worth presenting from two perspectives. One can verify that the solution to (2.1) for a limited set a, b is a power law multiplied by a log-periodic function, namely

$$f\,(x) = x^D \mathscr{G}\left(\frac{\log x}{\log a}\right), \tag{2.7}$$

where $\mathscr{G}\,(y) = \mathscr{G}\,(y + 1)$ and D is defined as in (2.3). Because the logarithm

action turns multiplication into addition, discrete self-similarity of a structure under stretching is the discrete *translational* symmetry of the logarithm of the structure.

On the other hand, one can approach the scaling of a function through its dimensionality. Generic objects such as lines and squares have the property that their topological and Hausdorff dimensions are equal, e.g. stretching the side of a 2d unit square to twice its length results in a square with area 2^2, indicative of a Hausdorff dimension 2. In fractals however, the topological dimension exceeds the Hausdorff one, e.g. the Sierpinski triangle has a one dimensional topology, but a Hausdorff dimension $\ln 3/\ln 2 \approx 1.585$. It is clear that the self-similarity is rooted in the dimensionality of the solution. In particular, DSI is associated with complex scaling exponents: The function $\mathscr{G}$ of (2.7) is periodic and consequently has a Fourier expansion,

$$\mathscr{G}(y) = \sum_{n=-\infty}^{\infty} c_n e^{i2\pi n y}, \tag{2.8}$$

so f has one as well,

$$f(x) = \sum_{n=-\infty}^{\infty} c_n x^{D+i\frac{2\pi n}{\ln a}}. \tag{2.9}$$

In a sense, f is a superposition of complex dimensional functions, with dimensions $D_n = (\ln b + i2\pi n)/\ln a$. If f were CSI, $\mathscr{G}$ would have been constant and there would be no complex exponents. We conclude that complex exponents are a signature of DSI.

2.1.2 Traditional substitution processes

Aperiodic and self similar structures such as fractals are often generated using iterative methods [26, 27]. A substitution process is also an iterative method, where one repeatedly applies an action on an existing structure to produce an infinite structure. Traditionally specified by an alphabet and a rule [28], the substitution process replaces "letters" in a sequence (tiles) by "words" (the rule), thereby inflating the original sequence. For the purposes of this work it suffices to consider a simple two-letter alphabet,

$$\{A, B\}, \tag{2.10}$$

and a general rule,

$$\sigma(A) = A^{n_1} B^{n_2}, \tag{2.11a}$$

$$\sigma(B) = A^{n_3} B^{n_4}, \tag{2.11b}$$

which for now applies to positive integers $n_{1,\dots,4}$, but will be generalized in section 2.1.3 to real numbers. Operating with σ on an initial sequence that is some combination of A, B, generates a longer sequence at each substitution step,

$$AB \to \sigma(AB) = \sigma(A)\,\sigma(B) = \underbrace{A\cdots}_{n_1}\underbrace{AB\cdots}_{n_2}\underbrace{BA\cdots}_{n_3}\underbrace{AB\cdots B}_{n_4} \to \cdots .$$

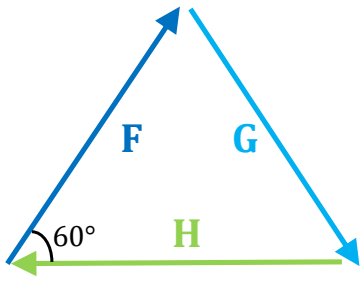

Figure 2.2: The substitution process that forms a Sierpinski triangle.

In physical applications, these letters represent e.g. atoms and molecules. Their density or order within the sequence corresponds to the sort of physical structure we would observe, be it a periodic lattice or an aperiodic one, e.g. the fractal Sierpinski triangle, formed by the substitution

$$\sigma(F) = FGFHF,$$

$$\sigma(G) = GG,$$

$$\sigma(H) = HH,$$

as shown in figure 2.2.

We associate with the letters *tiles* of type A, B, with respective lengths l_0^A, l_0^B. Denoting by l_n^i the accumulated length of tiles of type i in the sequence at substitution step n, rules (2.11) can be translated to an *occurrence matrix*

M, acting on a vector of lengths l_n. This occurrence matrix is chosen to be

$$M = \begin{pmatrix} n_1 & n_2 \\ n_3 & n_4 \end{pmatrix}, \tag{2.12}$$

specifying how the lengths of the A, B sub-tiles (words) evolve with each substitution step,

$$M \begin{pmatrix} l_n^A \\ l_n^B \end{pmatrix} = \begin{pmatrix} n_1 l_n^A + n_2 l_n^B \\ n_3 l_n^B + n_4 l_n^A \end{pmatrix} = \begin{pmatrix} l_{n+1}^A \\ l_{n+1}^B \end{pmatrix}. \tag{2.13}$$

M is insensitive to the order of letters in the rule. If we were to choose the rule $\sigma(A) = ABA$ instead of $\sigma(A) = AAB$, the resulting occurrence matrices are identical. It is beyond the scope of this work to discuss the implications of this feature.

The spectrum of M indicates how the lengths of sub-tiles A, B scale within finite segments of the infinite sequence. The eigenvector related to the leading (largest in absolute value) eigenvalue of M is

$$M \begin{pmatrix} \rho_A \\ \rho_B \end{pmatrix} = \lambda_1 \begin{pmatrix} \rho_A \\ \rho_B \end{pmatrix}, \tag{2.14}$$

where the eigenvectors are normalized to represent densities by demanding

$$\rho_A + \rho_B = 1. \tag{2.15}$$

$\rho_{A,B}$ are the asymptotic densities of tiles A, B within the infinite sequence M generates. They can be use to define a "lattice vector" for the infinite tile,

$$\overline{a} \equiv l_0^A \rho_A + l_0^B \rho_B. \tag{2.16}$$

For $n \gg 1$,

$$M^n \mathbf{l}_0 = |\lambda_1|^n \begin{pmatrix} \rho_A \\ \rho_B \end{pmatrix} + \mathcal{O}\left(|\lambda_2|^n\right), \tag{2.17}$$

where $|\lambda_1| \geq |\lambda_2|$ are the eigenvalues of M. We also define the length of the sub-sequence with a total of k tiles,

$$x(k) = l_0^A m_A(k) + l_0^B m_B(k), \tag{2.18}$$

where $m_i(k)$ are the numbers of $i = \{A, B\}$ type tiles within this k-long subsequence. Taking the limit of infinite n (infinite k) of $x(k)$, it follows that

$$\lim_{k(n)\to\infty} \frac{x(k)}{k} = \overline{a}. \tag{2.19}$$

This asymptotic relation allows us to define $u(k)$, the fluctuation of $x(k)$ from a lattice with a unit cell of length a, namely

$$x(k) = \overline{a}k + u(k). \tag{2.20}$$

Recall $k = k(n)$. From (2.18) it follows that x is the L_1 norm of the length of the tiling, namely

$$|M^n \mathbf{l}_0|_1 = x(k). \tag{2.21}$$

Combining equations (2.21) and (2.20), it follows that the asymptotic scaling of $k, u(k)$ are

$$k \sim |\lambda_1|^n, \tag{2.22}$$

$$u(k) \sim |\lambda_2|^n. \tag{2.23}$$

When scaling $u(k) \to u(\lambda k)$ and substituting $n = \ln k / \ln \lambda_1 + \mathcal{O}(\ln \lambda_2 / \ln \lambda_1)$ into equation (2.23), one obtains

$$u(\lambda k) \sim \lambda_2^{\frac{\ln k + \ln \lambda}{\ln \lambda_1}} = \lambda_2^{\frac{\ln \lambda}{\ln \lambda_1}} u(k). \tag{2.24}$$

The specific choice $\lambda = \lambda_1^D$, where D is the Hausdorff dimension defined in equation (2.3), we have

$$u\left(\lambda_1^D k\right) \sim \lambda_2^D u(k). \tag{2.25}$$

We recover the scaling of equation (2.1) and thus reveal the asymptotic DSI of $u(k)$, as equation (2.25) is only satisfied for the set $\{\lambda_1, \lambda_2\}$. The most general form of $u(k)$ in an infinite tiling is then [29]

$$u(k) \sim k^D F\left(\frac{\ln k}{\ln \lambda_1}\right), \tag{2.26}$$

where F is a log-periodic function, namely $F(x+1) = F(x)$. Asymptotically, M generates either exactly periodic, quasi-periodic or fractal tilings, depending on the scaling of $u(k)$.

2.1.3 Generalized tilings

Generalizing to a non-integer, non-positive substitution process [12], one defines the rule

$$\sigma(A) = A^{a_1} B^{b_1}, \tag{2.27a}$$

$$\sigma(B) = A^{a_2} B^{b_2}, \tag{2.27b}$$

where now, in contrast with (2.11), a_i, b_i are real numbers. Instead of a set of tiles, the concept of "filling" a background unit cell structure with constant potentials V_A, V_B is chosen. The Integer part of a_i, b_i determines how many unit cells will be completely filled with V_A, V_B, respectively. The non integer part determines what fraction of the $\mathrm{Int}(a_i) + 1$ cell is filled with either potential. Similarly, we replace the lengths of sub-tiles l_n^i with another measure – the work a particle with some "charge" exerts while moving through the potential signature of the sequence. In a two-letter substitution with k letters, the work done by a such a particle is

$$W_j(k) = q \int_0^k V_j(x)\, dx, j \in \{A, B\}. \tag{2.28}$$

The potentials are constant, so the total work is

$$W_j(k) = q V_j l_j(k). \tag{2.29}$$

(2.29) provides meaning to negative powers that were made possible in (2.27); One fills the cell with the negative of the potential in question and negative contributions to the work cancels positive ones. In the generalized case, however, M is not guaranteed to be diagonalizable. For a given M that is, the results of section 2.1.2 still hold.

2.2 Fractal properties of Efimov physics

Although substitutions are intuitively relevant to geometrical structures, there is much to be gained by relating them to other physical quantities. In what follows, we present a mapping of the Efimov RG flow to substitutions, and extract visual representations of energy levels as fractal, periodic and aperiodic tilings.

The original derivation of the Efimov effect [30] involved the low energy states of three identical, spinless particles, whose pair-wise interactions' range r_0 vanishes and scattering length in the s-channel a_0 is infinite. The three-body problem is reduced to an effective two-body problem with an inverse-square potential. The magnitude of the potential is independent of the precise details of the interactions. With the lack of a characteristic scale in the problem, and despite being unable to form pair-wise bound states, a universal geometric spectrum of three-body bound states arises. The effective interaction Efimov found is [17]

$$V_{\text{eff}}(R) = -\frac{|s_0|^2 + 1/4}{R^2}, \tag{2.30}$$

where $|s_0| \simeq 1.006$ is universal. The Efimov spectrum then obeys the scaling relation $E_n = e^{-2\pi n/|s_0|} E_0$.

The famous fractal spectrum is recovered as a limit of the $1/r^2$ potential Schrödinger equation. This equation is scale free by virtue of the shared inverse-square scaling of the kinetic and potential terms. A quantum ground state can only be obtained by implementing a cutoff that breaks the CSI of the equation, resulting in this continuous symmetry being broken into a discrete self-similar spectrum of bound states that converges to zero,

$$E_n = E_0 e^{-\frac{2\pi}{\sqrt{\xi - \xi_c}} n},$$

for any $n \in \mathbb{N}$. These bound states are only obtained for dimensionless amplitudes ξ of the inverse-square interaction that are strictly greater than $\xi_c = (2-d)^2/4$. In three dimensions $\xi_c = 1/4$, and it follows that when $\xi = |s_0|^2 + 1/4$, the $1/r^2$ Schrödinger equation precisely replicates the fractal Efimov spectrum.

A direct consequence of the effective approach is a RG flow with phases of either fixed points or limit cycle solutions, depending on the critical value ξ_c. While the fixed points stand for other, CSI solutions to the Schrödinger equa-

tion, the limit cycles correspond to the fractal Efimov bound states, motivating us to explore these periodic solutions using substitution tilings.

2.2.1 Schrödinger equation approach

Before taking the limits appropriate for Efimov bound states, we begin with the inverse-square potential Schrödinger equation ($\hbar = 1$),

$$-\left(\frac{1}{2\mu}\nabla^2 + \frac{\zeta}{r^2}\right)\psi\left(\mathrm{r}\right) = E\psi\left(\mathrm{r}\right). \tag{2.31}$$

This Hamiltonian is highly singular at $r = 0$ and consequently not self-adjoint and unphysical. The equation is scale free: (2.31) is invariant under the transformation $r \to \lambda r,\ E \to \lambda^{-2}E$ for any λ. In fact, the only parameter $2\mu\zeta$ is dimensionless, resulting in (2.31) being CSI. It follows that a consequence of a single bound state $\{E_n, \psi_{nlm}\left(r, E_n\right)\}$ is an unbounded from below continuum of bound states $\left\{\lambda E_n, \psi_{nlm}\left(\lambda r, E_n\lambda^{-2}\right)\right\}$, and a "ground state" at negative-infinite energy. This is caused by the strongly singular interaction. To be able to obtain the Efimov bound states, the Hamiltonian would require regularization. In spherical coordinates, one recognizes the radial and angular contributions to the Laplacian,

$$\nabla^2 = \frac{1}{r^2}\partial_r\left(r^2\partial_r\right) + \frac{1}{r^2}\left(\frac{1}{\sin\theta}\partial_\theta\left(\sin\theta\partial_\theta\right) + \frac{1}{\sin^2\theta}\partial_\phi^2\right), \tag{2.32}$$

which begs the introduction of an appropriate separation of variables,

$$\psi_{nlm}\left(\mathrm{r}\right) = \frac{1}{r}\chi_{nl}\left(r\right)Y_l^m\left(\theta,\phi\right). \tag{2.33}$$

Inserting (2.32) and (2.33) into (2.31) and rearranging, we find the separated equation

$$r^2\frac{\chi_{nl}''\left(r\right)}{\chi_{nl}\left(r\right)} + 2\mu r^2\left(E - \frac{\zeta}{r^2}\right) = \frac{\hat{L}^2Y_l^m\left(\theta,\phi\right)}{Y_l^m\left(\theta,\phi\right)}. \tag{2.34}$$

The r.h.s is a simple eigenvalue equation for the angular momentum operator,

$$\hat{L}^2Y_l^m\left(\theta,\phi\right) = l\left(l+1\right)Y_l^m\left(\theta,\phi\right). \tag{2.35}$$

Combining equations (2.34) and (2.35), one obtains the radial equation

$$\chi_{nl}''\left(r\right) + \left(-2\mu\frac{\zeta}{r^2} + \frac{l\left(l+1\right)}{r^2}\right)\chi_{nl}\left(r\right) = 2\mu E\chi_{nl}\left(r\right). \tag{2.36}$$

Generalizing to d-dimensions, the hyperradial Schrödinger equation is

$$\chi''_{nl}(r) + \frac{d-1}{r}\chi'_{nl}(r) + \left(\frac{\xi}{r^2} - k^2\right)\chi_{nl}(r) = 0, \tag{2.37}$$

with $\xi = 2\mu\zeta - l(l+d-2), k^2 = -2\mu E$.

To force self-adjointness on the Hamiltonian we introduce a short distance cutoff. At $r = L_0$ we impose some short-range interaction, whose explicit form is irrelevant and with the general boundary condition [9, 21]

$$g(L_0) \equiv \frac{L_0\chi'_{nl}(L_0)}{\chi_{nl}(L_0)}. \tag{2.38}$$

This boundary condition immediately breaks the CSI, forcing a characteristic length scale L_0. The Hamiltonian becomes self-adjoint and equation (2.37) now has well defined solutions. To recover the s-wave bound states of Efimov, we consider the radial wave-function with $E < 0$ and $l = 0$,

$$\chi(r) = r^{-\sqrt{\xi_c}}\left(a_1 J_{\sqrt{\xi_c-\xi}}(-ikr) + a_2 Y_{\sqrt{\xi_c-\xi}}(-ikr)\right), \tag{2.39}$$

where $J_n(x), Y_n(x)$ are Bessel functions of the first and second kind, and

$$\xi_c = \frac{(d-2)^2}{4}. \tag{2.40}$$

We expect to recover Efimov bound states in the low energy limit $kL_0 \ll 1$. The radial solution to leading order in kr is [31, 32]

$$\chi(r) \approx a_1 k^{\sqrt{\xi_c-\xi}} r^{-\sqrt{\xi_c}+\sqrt{\xi_c-\xi}} + a_2 k^{-\sqrt{\xi_c-\xi}} r^{-\sqrt{\xi_c}-\sqrt{\xi_c-\xi}}. \tag{2.41}$$

For $\xi \leq \xi_c$, inserting (2.41) into (2.38) gives

$$g(L_0) = -\sqrt{\xi_c} - \sqrt{\xi_c - \xi}, \tag{2.42}$$

and the corresponding energy levels when $E \simeq 0$ are

$$E = -\frac{\mathscr{F}(g,\xi)}{2\mu L_0^2},$$

and are CSI. For $\xi > \xi_c$ however, outside the boundary at $r = L_0$ we have

$$(kL_0)^{2i\sqrt{\xi-\xi_c}} = e^{i\varphi}, \tag{2.43}$$

where φ is some phase whose explicit form is irrelevant. Solving for the energy levels, we obtain the Efimov geometric series of bound states,

$$k_n = k_0 e^{\frac{\pi}{\sqrt{\xi-\xi_c}} n}, n \in \mathbb{Z}, \tag{2.44}$$

with $k_0 = e^{\varphi/2}\sqrt{\xi-\xi_c}/L_0$. The bound states in this limit have the same form of the DSI spectrum of Efimov physics when the branch $n \leq 0$ is chosen.

2.2.2 Renormalization group approach

In the previous subsection, our derivation resulted in a phase transition of the short range coupling g from a constant function to an oscillatory one as ξ increases above ξ_c. One expects such a transition to be present in an RG flow that describes this system. Our goal is to obtain this RG flow and investigate the critical behavior of g as a function of ξ.

For a ξ/r^2 potential, ξ is dimensionless and using RG is not as useful ((2.37) is scale free). To overcome this obstacle, we temporarily replace the inverse square potential by ξ/r^s and take $s \to 2$ when we are done.

Introducing a scale parameter $L_0 \leq L < \infty$, dimensional analysis determines

$$\xi = \xi_0 L^{s-2}. \tag{2.45}$$

The β function for ξ is obtained by taking the derivative of (2.45) with respect to $\ln L$,

$$\beta_\xi \equiv L\frac{d\xi}{dL} = (s-2)\,\xi. \tag{2.46}$$

Combining (2.37) and (2.38) in the low energy limit, it follows that the beta function for g is [21, 32]

$$\beta_g \equiv L\frac{dg}{dL} = (2-d)\,g - g^2 - L^{2-s}\xi. \tag{2.47}$$

The RG equations for $s = 2$ are then

$$L\frac{d\xi}{dL} = 0, \tag{2.48a}$$

$$L\frac{dg}{dL} = (2-d)\,g - g^2 - \xi. \tag{2.48b}$$

Taking $\beta_g = 0$ gives the fixed points of (2.48b),

$$g_{\pm} = -\sqrt{\xi_c} \pm \sqrt{\xi_c - \xi}, \tag{2.49}$$

with ξ_c given in (2.40).

Let us first consider $\xi < \xi_c$. In this regime, the fixed points $g_{\pm}$ are real. As ξ approaches ξ_c, the two fixed points merge into a single one, $g^* = -\sqrt{\xi_c}$ at $\xi = \xi_c$ [31]. For $\xi > \xi_c$ the fixed points are complex. We solve for g by integrating both sides of (2.48b). Then,

$$g(L) = -\sqrt{\xi_c} - \sqrt{\xi - \xi_c} \tan\left(\sqrt{\xi - \xi_c} \ln\left(\frac{L}{L_0}\right) - C\right), \tag{2.50}$$

with $C = \tan^{-1}\left(\left(g_0 - \sqrt{\xi_c}\right)/\sqrt{\xi - \xi_c}\right)$. The solution in (2.50) is obviously periodic, pointing of a limit cycle solution with period

$$g(L) = g\left(e^{\frac{n\pi}{\sqrt{\xi - \xi_c}}} L\right). \tag{2.51}$$

(2.51) exhibits log-periodic self similarity,

$$g(\ln L) = g\left(\ln L + \frac{n\pi}{\sqrt{\xi - \xi_c}}\right). \tag{2.52}$$

As discussed in 2.1.1, we find that g is a fractal for $\xi > \xi_c$.

2.2.3 Mapping Efimov physics to a substitution process

Let us now demonstrate how the scaling of the coupling g in both $\xi \leq \xi_c, \xi > \xi_c$ regimes manifests as substitution tilings.

We define the scaling parameter

$$\ln L \equiv k, \tag{2.53}$$

as well as the coupling,

$$g(\ln L) \equiv g_k \equiv \frac{l_k^A}{l_k^B}, \tag{2.54}$$

with l_k^A, l_k^B the lengths of sub-tilings of type A, B at step k of the substitution. Mapping (2.48b) to a substitution tiling will require a discretized evolution equation, because the substitution process is a discrete map. At the fixed points

$g_{k+1} = g_k$ and $g_k^2 = g_{k+1}g_k$. Inserting (2.54) into a discretized (2.48b) yields

$$(2-d)\, g_k - g_{k+1}g_k - \xi = 0. \tag{2.55}$$

Combining (2.55) and (2.54), the flow can be expressed in terms of l_A, l_B,

$$\frac{l_{k+1}^A}{l_{k+1}^B} l_k^A = (2-d)\, l_k^A - \xi l_k^B. \tag{2.56}$$

We define the **mapping** [12]:

$$\frac{l_k^A}{l_k^B} \mapsto \begin{pmatrix} l_k^A \\ l_k^B \end{pmatrix}, \tag{2.57}$$

under which equation (2.56) becomes the ratio of a set recursion rules,

$$l_{k+1}^A = (2-d)\, l_k^A - \xi l_k^B, \tag{2.58a}$$
$$l_{k+1}^B = l_k^A. \tag{2.58b}$$

Equations (2.58) are associated with an occurrence matrix

$$\mathbf{l}_{k+1} = C \begin{pmatrix} 2-d & -\xi \\ 1 & 0 \end{pmatrix} \mathbf{l}_k \equiv M \mathbf{l}_k, \tag{2.59}$$

and as demonstrated in section 2.1.3, it defines the two-letter alphabet substitution process

$$A \mapsto A^{(2-d)} B^{-\xi}, \tag{2.60a}$$
$$B \mapsto A. \tag{2.60b}$$

The spectrum of M is then

$$\mathrm{spec}\,(M) = \left\{ -\sqrt{\xi_c} + \sqrt{\xi_c - \xi}, -\sqrt{\xi_c} - \sqrt{\xi_c - \xi} \right\}, \tag{2.61}$$

consisting of the fixed points of equation (2.49).

2.2.4 Fixed points

Any fixed point of $g(\ln L)$ satisfies $g_k = g_{k'}$, namely

$$\frac{l_k^A}{l_k^B} = \frac{l_{k'}^A}{l_{k'}^B} \quad \forall k, k'.$$

It follows that an eigenvector of M corresponds to a fixed point of g. For $\xi < \xi_c$, the two fixed points in equation (2.49) coincide with the ratio of the normalized eigenvectors $\tilde{l}_{1,2}$ and one finds $\tilde{l}_i^A/\tilde{l}_i^B = g_\pm$ $(i = 1, 2)$. Where $\xi = \xi_c$, (2.59) has a single eigenvalue $g^* = -\sqrt{\xi_c}$, with eigenvectors that satisfy $l_i^{A*}/l_i^{B*} = -\sqrt{\xi_c}$.

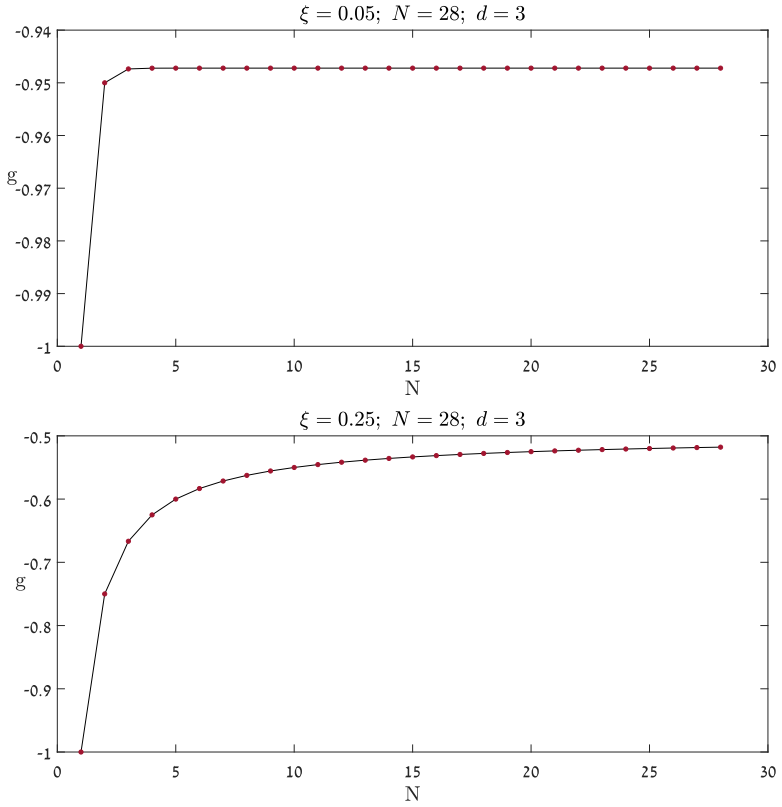

Figure 2.3: For $d = 3$, $\xi = 0.05$ (top) and $\xi = 0.25$ (bottom) the coupling g converges to the fixed points $g_{0.05} \approx -0.95, g_{0.25} = -0.5$ over N runs of the substitution.

Figures 2.4-(2.5) display the 2-dimensional visualization of the two-letter tilings corresponding to the rules (2.60) for $d = 3$. l_A, l_B are the lengths of tiles of type A, B, respectively, throughout the sequence. The interpretation of eigenvectors as fixed points is established by comparing the evolution of the

sequences and the coupling g. In figure 2.4, the sequences begin with some initial condition and soon assume completely periodic evolution, consistent with the Efimov $\xi \leq \xi_c$ regime. g converges to the stable fixed point at $\xi = 0.25$, as seen in figure 2.3, indicative of the link between the periodicity of a tiling and a fixed point of the flow.

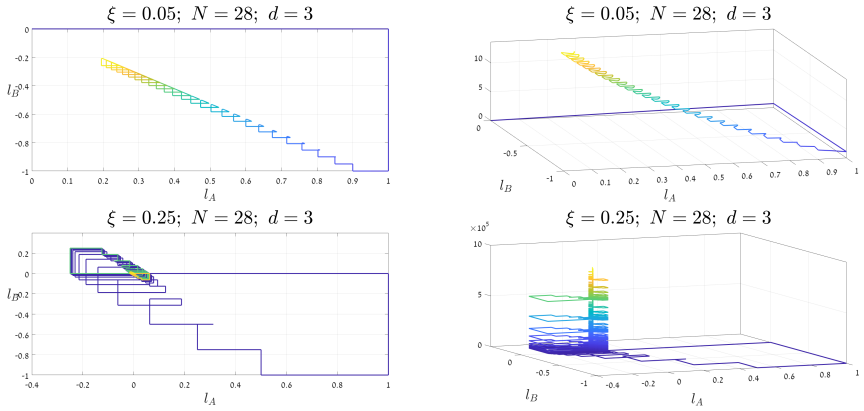

Figure 2.4: For $d = 3$, the mapped sequence of $\xi = 0.05$ (top) and $\xi = 0.25$ (bottom) evolves periodically, with $N = 28, 30$ substitution steps done to obtain the tiles, respectively.

2.2.5 Limit Cycle solutions

For $\xi > \xi_c$, consider some initial condition decomposed into a linear combination of the spanning eigenvectors of M,

$$\mathbf{l}_{k_0} = A\tilde{\mathbf{l}}_1 + B\tilde{\mathbf{l}}_2. \tag{2.62}$$

We apply the substitution (2.59) n times, which transforms (2.62) into

$$M^n \mathbf{l}_{k_0} = \lambda_1^n A\tilde{\mathbf{l}}_1 + \lambda_2^n B\tilde{\mathbf{l}}_2. \tag{2.63}$$

For $M_{ij} \in \mathbb{R}$ with complex eigenvalues $\lambda_1 = \lambda_2^*$, the amplitude can be taken out,

$$M^n \mathbf{l}_{k_0} = |\lambda_1|^n \left(A\tilde{\mathbf{l}}_1 e^{in\Theta} + B\tilde{\mathbf{l}}_2 e^{-in\Theta} \right). \tag{2.64}$$

One discovers that whenever $n = -n + 2\pi m/\Theta$ for $m \in \mathbb{Z}$, the vector (2.63) is recovered up to a stretch. A global multiplicative constant does not affect the

ratio of the vector's components, namely $g_k = g_{k_0}$ if and only if

$$k = k_0 + \frac{\pi m}{\Theta}. \tag{2.65}$$

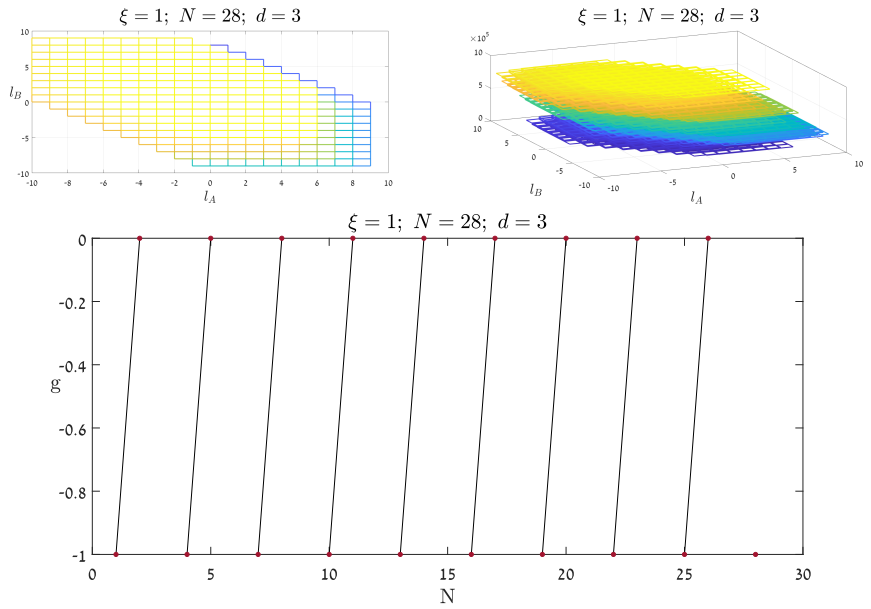

Figure 2.5: For $d = 3$, $\xi = 1$, the tiling formed by the mapping is a fractal (top). g follows a limit cycle with a discrete period (bottom)

For $M_{ij} \in \mathbb{C}$, the largest (in absolute value) eigenvalue dominates the evolution of the sequence. For $n \gg 1$ and $|\lambda_1| > |\lambda_2|$ without loss of generality, we repeat the process of equation (2.64) and obtain

$$M^n \mathbf{l}_{k_0} = |\lambda_1|^n \left(A\tilde{\mathbf{l}}_1 e^{in\Theta} + \left|\frac{\lambda_2}{\lambda_1}\right|^n B\tilde{\mathbf{l}}_2 e^{-in\Theta'} \right) \sim A\,|\lambda_1|^n\, \tilde{\mathbf{l}}_1 e^{in\Theta}. \tag{2.66}$$

The same argument of the complex conjugate eigenvalues applies for a sufficiently large n. Any $n' = n + 2\pi m/\Theta$ for $m \in \mathbb{Z}$ recovers nearly the same tiling with increasing accuracy, up to an exponentially suppressed correction,

$$M^{n'} \mathbf{l}_{k_0} = |\lambda_1|^{\frac{2\pi}{\Theta} m}\, M^n \mathbf{l}_{k_0} + \mathcal{O}\left(\left|\frac{\lambda_2}{\lambda_1}\right|^{n + \frac{2\pi}{\Theta} m} \right). \tag{2.67}$$

The tiling equation (2.67) is quasi-periodic, its DSI recovered only in the limit $n \to \infty$.

The discrete-periodic orbits of sequences (2.64) and (2.67) are limit cycles of g_k. Where $\xi > \xi_c$, the complex eigenvalues of M in equation (2.61) correspond to $\Theta = \arctan\left(\sqrt{(\xi - \xi_c)/\xi_c}\right)$. Close to the critical point, $\xi - \xi_c \ll 1$ and

$$\Theta \approx \sqrt{(\xi - \xi_c)/\xi_c}. \tag{2.68}$$

The scale invariance of g then follows from equation (2.65),

$$g(\ln L) = g\left(\ln L_0 + \frac{\pi m\sqrt{\xi_c}}{\sqrt{\xi - \xi_c}}\right). \tag{2.69}$$

In 3 dimensions, the critical point is

$$\xi_c = 0.25, \tag{2.70}$$

and when $m = 4, 8, 16, \ldots$ the factor $\sqrt{\xi_c}$ is absorbed to form an integer, recovering the scaling of the limit cycle from equation (2.52).

In figure 2.5, the limit cycle of g is obtained when $\xi = 1$ and manifests as a *self-similar* tiling. When $\xi = 2$, g is self-similar with aperiodic scaling, and the tiling associated with it is also an aperiodic tiling (see figure 2.6).

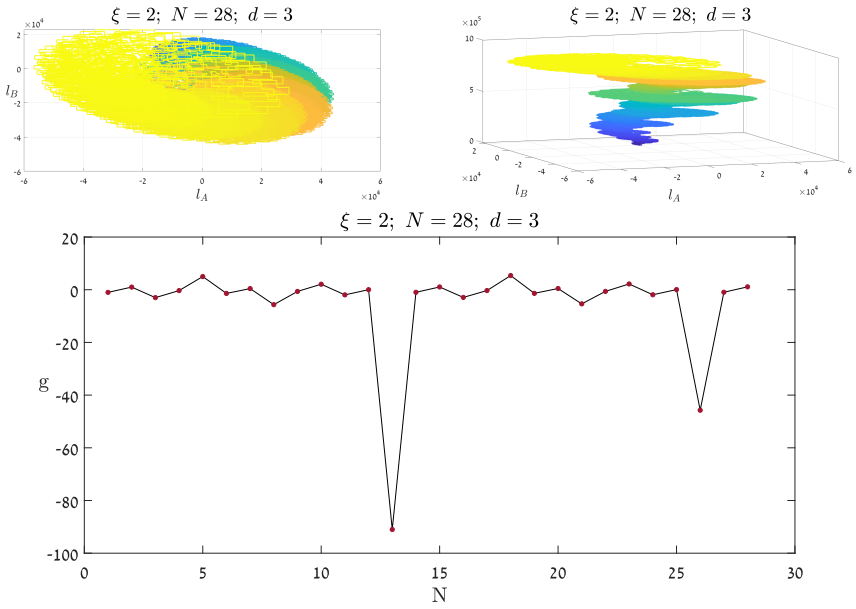

Figure 2.6: For $d = 3$, $\xi = 2$, the tiling formed by the mapping is aperiodic (top). g is self similar with slight inconsistencies (bottom).

2.2.6 Mapping quadratic RG flows to a substitution tiling

Having tested the mapping on the Efimov RG flow, we reformulate the results of section 2.2.3 to suit a wider variety of flows. In particular, any system which has a single β function for a single coupling u, of the form

$$\partial_t u = Au^2 + Bu + C, \tag{2.71}$$

can undergo the Efimov mapping [12]. The occurrence matrix extracted from equation (2.71) is

$$M = \begin{pmatrix} -\frac{B}{A} & -\frac{C}{A} \\ 1 & 0 \end{pmatrix}. \tag{2.72}$$

If M is diagonalizable, its eigenvalues are

$$\lambda_\pm = \frac{-B \pm \sqrt{B^2 - 4AC}}{2A}, \tag{2.73}$$

with normalized eigenvectors

$$\begin{pmatrix} v_1^\pm \\ v_2^\pm \end{pmatrix} = \frac{1}{1+\lambda_\pm} \begin{pmatrix} \lambda_\pm \\ 1 \end{pmatrix}, \tag{2.74}$$
$$v_1 + v_2 = 1.$$

By the same argument of section 2.2.4, for real A, B, C and $4AC \leq B^2$, the eigenvalues are also real and $\lambda_\pm$ are the fixed points of the flow in equation (2.71). If A, B or C are complex, or if they are real and $4AC > B^2$, limit cycles emerge due to complex fixed points of M. We also note that when $C = 0$, the substitution process is degenerate; Either it generates a completely periodic, one-letter sequence, or it annihilates the initial sequence entirely.

3 Fractal spacetimes in Quantum Einstein gravity

Although these two theories certainly seem unrelated, the investigation of Efimov physics under the mapping was designed to grant insight on the flow of Quantum Einstein Gravity. The following reveals that they exhibit similar behaviors as substitution processes. Their limit cycle solutions, while quite different, hint at some deeper connection.

QEG is unique among quantum gravity theories in its formulation. Its effective approach pushes the probing scale deeper into the UV without encountering the usual infinities; Instead, there emerges an exotic, self-similar universe as one approaches the Planck scale. At the center of the effective theory lies the average (scale dependent) effective action Γ_k. By using exact renormalization group, one finds that this action evolves according to a Wetterich flow equation of the form (A.15)

$$\partial_t \Gamma_k = \frac{1}{2} \mathrm{Tr} \left(\frac{\partial_t R_k}{\Gamma_k^{(2)} + R_k} \right).$$

From this flow one is able to extract the flow of the gravitational and cosmological couplings. Their flows exhibit limit cycles, which translate to DSI correlation functions with a scaling relation

$$\mathcal{G}^{(n)} \left(e^T x; g_k, \Lambda_k, k \right) = \mathcal{G}^{(n)} \left(x, g_k, \Lambda_k \right).$$

Because the QEG spacetime has a limit cycle, we are able to probe this unusual structure with our method. In the previous part of this work we defined a mapping of quadratic RG flows, and while the RG flow of QEG turns out much less simple to handle, we are able to extract a quadratic equation that relates g_k, Λ_k. As we did in Efimov Physics, mapping this equation to a substitution process results in fractal tilings corresponding to the limit cycles.

3.1 The formulation of QEG

In any quantum field theory (QFT), one seeks an appropriate gauge group. In gravity, a theory must be invariant under diffeomorphisms, or coordinate transformations of the metric. Unfortunately, if one wishes to find a QFT which explains and predicts gravity, it cannot presuppose a metric, let alone one which is well behaved and causal. How does one produce a covariant formulation of a theory where the quantum field is a metric?

Quantum Einstein Gravity overcomes this fundamental issue by using the background-field gauge [1]. The gravitational field is split into two metrics,

$$\gamma_{\mu\nu}(x) = \overline{g}_{\mu\nu}(x) + h_{\mu\nu}(x), \tag{3.1}$$

where $h_{\mu\nu}$ is a dynamical, fluctuating field and $\overline{g}_{\mu\nu}$ is a fixed, completely *arbitrary* background metric. Throughout the formulation, one can verify that no observable quantity may ever depend on $\overline{g}_{\mu\nu}$. Diffeomorphism invariance means the gravitational action is invariant under the coordinate transformation

$$\delta\gamma_{\mu\nu} = \mathcal{L}_v \gamma_{\mu\nu}, \tag{3.2}$$

where $\mathcal{L}_v$ is the Lie derivative with respect to the vector field v. The particular background-field gauge

$$\delta h_{\mu\nu} = \mathcal{L}_v h_{\mu\nu}, \quad \delta\overline{g}_{\mu\nu} = \mathcal{L}_v \overline{g}_{\mu\nu}, \tag{3.3}$$

is chosen to guarantee a diffeomorphism invariant *effective action.* Combining the background gauge and the Wetterich equation discussed in appendix A allows QEG to overcome the traditional non-renormalizability of quantum gravity and obtain a RG flow equation of the couplings.

3.1.1 Construction of the effective action for gravity

The standard form of the generating functional for connected correlation functions, with the modification of scale dependence (see appendix A), is [1]

$$W_k\left[t^{\mu\nu},\sigma^{\mu},\overline{\sigma}_{\mu};\overline{g}_{\mu\nu}\right]=\ln\left\{\int\mathcal{D}h\mathcal{D}C\mathcal{D}\overline{C}\exp\left[-S\left[\overline{g}+h\right]-S_{\mathrm{gf}}\left[h;\overline{g}\right]\right.\right. \tag{3.4}$$
$$\left.\left.-S_{\mathrm{gh}}\left[h,C,\overline{C};\overline{g}\right]-\Delta S_k\left[h,C,\overline{C};\overline{g}\right]-S_{\mathrm{source}}\right]\right\},$$

where the various terms in the action are discussed below. The usual spacetime integration is replaced by the diffeomorphism invariant measure

$$\int d^dx\sqrt{\overline{g}},$$

with $g\equiv\det g_{\mu\nu}$. S is the classical action, invariant under the general coordinate transformation

$$\delta\gamma_{\mu\nu}=\mathcal{L}_{\upsilon}\gamma_{\mu\nu}\equiv\upsilon^{\rho}\partial_{\rho}\gamma_{\mu\nu}+\partial_{\mu}\upsilon^{\rho}\gamma_{\rho\nu}+\partial_{\nu}\upsilon^{\rho}\gamma_{\mu\rho}, \tag{3.5}$$

with a ghost action

$$S_{\mathrm{gh}}\left[h,C,\overline{C};\overline{g}\right]=-\kappa^{-1}\int d^dx\sqrt{\overline{g}}\overline{C}_{\mu}\mathcal{M}\left[g,\overline{g}\right]^{\mu}{}_{\nu}C^{\nu}, \tag{3.6}$$

where $\kappa=\left(32\pi\overline{G}\right)^{-1/2}$, $\overline{G}$ the bare Newton's constant and $g\equiv\overline{\gamma}$ the expectation value of the complete metric. $\mathcal{M}$ is obtained from the gauge fixing condition, using the usual Fadeev-Popov procedure. The coordinate transformation

$$\delta C^{\mu}=\mathcal{L}_{\upsilon}C^{\mu},\quad\delta\overline{C}_{\mu}=\mathcal{L}_{\upsilon}\overline{C}_{\mu}, \tag{3.7}$$

combined with the metric transformation (3.3) leaves the full action invariant. The action is equipped with a source term

$$S_{\mathrm{source}}=-\int d^dx\sqrt{\overline{g}}\left\{t^{\mu\nu}h_{\mu\nu}+\overline{\sigma}_{\mu}C^{\mu}+\sigma^{\mu}\overline{C}_{\mu}\right\} \tag{3.8}$$

and a gauge fixing term,

$$S_{\mathrm{gf}}\left[h;\overline{g}\right]=\frac{1}{2\alpha}\int d^dx\sqrt{\overline{g}}\overline{g}^{\mu\nu}F_{\mu}F_{\nu}, \tag{3.9}$$

with gauge fixing condition $F_{\mu}\left(\overline{g},h\right)=0$, specified later in section 3.2.1. The IR cutoff action is defined both for the metric and the ghosts in a quadratic

form,

$$\Delta S_k = \frac{\kappa^2}{2}\int d^dx\sqrt{\overline{g}}h_{\mu\nu}\left(R_k^{\text{grav}}\left[\overline{g}\right]\right)^{\mu\nu\rho\sigma}h_{\rho\sigma} + \sqrt{2}\int d^dx\sqrt{\overline{g}}\overline{C}^{\mu}R_k^{\text{gh}}\left[\overline{g}\right]^{\mu}{}_{\nu}C^{\nu}. \tag{3.10}$$

$R_k^{\text{gh}}\left[\overline{g}\right], R_k^{\text{grav}}\left[\overline{g}\right]$ discriminate between high and low eigenmodes of $-\overline{D}^2 = -\overline{g}^{\mu\nu}\overline{D}_\mu\overline{D}_\nu$. The use of the energy scale of an external background field, rather than the full metric, is chosen in order to keep the suppressing action quadratic in $h_{\mu\nu}$. This is crucial to guarantee that the flow equation formulated in appendix A involves no higher than second-order derivatives of the effective action.

The clever choice of a background gauge guarantees that the generating functional is invariant under any coordinate transformation,

$$\begin{aligned} W_k\left[t^{\mu\nu}+\mathcal{L}_v t^{\mu\nu}, \sigma^\mu+\mathcal{L}_v\sigma^\mu, \overline{\sigma}_\mu+\mathcal{L}_v\overline{\sigma}_\mu; \overline{g}+\mathcal{L}_v\overline{g}\right] \\ = W_k\left[t^{\mu\nu}, \sigma^\mu, \overline{\sigma}_\mu; \overline{g}\right]. \end{aligned} \tag{3.11}$$

It contains only scalar (diffeomorphism invariant) quantities because indices were contracted using the background field, which transforms under the gauge-transformation (3.3) as well.

3.1.2 The average effective action - formulation and flow

To obtain the effective action $\tilde{\Gamma}_k$, we begin by taking the derivative of W_k w.r.t the sources,

$$\overline{h}_{\mu\nu} = \frac{1}{\sqrt{\overline{g}}}\frac{\delta W_k}{\delta t^{\mu\nu}}, \qquad \xi^\mu = \frac{1}{\sqrt{\overline{g}}}\frac{\delta W_k}{\delta \overline{\sigma}_\mu}, \qquad \overline{\xi}_\mu = \frac{1}{\sqrt{\overline{g}}}\frac{\delta W_k}{\delta \sigma^\mu}. \tag{3.12}$$

The Legendre transform then reads

$$\tilde{\Gamma}_k\left[\overline{h}, \xi, \overline{\xi}; \overline{g}\right] = \int d^dx\sqrt{\overline{g}}\left\{t^{\mu\nu}\overline{h}_{\mu\nu} + \overline{\sigma}_\mu\xi^\mu + \sigma^\mu\overline{\xi}_\mu\right\} - W_k\left[t, \sigma, \overline{\sigma}; \overline{g}\right]. \tag{3.13}$$

The effective average action is then obtained as in (A.12) by

$$\Gamma_k\left[\overline{h}, \xi, \overline{\xi}; \overline{g}\right] = \tilde{\Gamma}_k\left[\overline{h}, \xi, \overline{\xi}; \overline{g}\right] - \Delta S_k\left[\overline{h}, \xi, \overline{\xi}; \overline{g}\right]. \tag{3.14}$$

Under (3.3) and (3.7), it is invariant on-shell (its arguments are on-shell quantities),

$$\Gamma_k\left[\overline{h}+\mathcal{L}_v\overline{h},\xi+\mathcal{L}_v\xi,\overline{\xi}+\mathcal{L}_v\overline{\xi};\overline{g}+\mathcal{L}_v\overline{g}\right]=\Gamma_k\left[\overline{h},\xi,\overline{\xi};\overline{g}\right]. \tag{3.15}$$

The functional RG equation is taken w.r.t all fields in the argument of Γ_k, namely gravitons and ghosts. The Wetterich equation for QEG is then

$$\partial_t\Gamma_k=\mathrm{Tr}\left\{\frac{1}{2}\left(\Gamma_k^{(2)}+\hat{R}_k\right)^{-1}_{\overline{hh}}\left(\partial_t\hat{R}_k\right)_{\overline{hh}}-\left(\Gamma_k^{(2)}+\hat{R}_k\right)^{-1}_{\overline{\xi}\xi}\left(\partial_t\hat{R}_k\right)_{\overline{\xi}\xi}\right\}, \tag{3.16}$$

with

$$\Gamma_k^{(2)ij}(x,y)\equiv\frac{1}{\sqrt{\overline{g}(x)\,\overline{g}(y)}}\frac{\delta^2\Gamma_k}{\delta\varphi_i(x)\,\delta\varphi_j(y)},\quad \varphi\equiv\left\{\overline{h}_{\mu\nu},\xi^\mu,\overline{\xi}_\mu\right\}$$

and

$$\left(\hat{R}_k^{\mu\nu\rho\sigma}\right)_{\overline{hh}}\equiv\kappa^2\left(R_k^{\mathrm{grav}}\left[\overline{g}\right]\right)^{\mu\nu\rho\sigma},\qquad\left(\hat{R}_k\right)_{\overline{\xi}\xi}\equiv\sqrt{2}R_k^{\mathrm{gh}}\left[\overline{g}\right].$$

In the case of gravity, the trace includes spacetime integration over the invariant measure $\int d^dx\sqrt{\overline{g}}$.

3.1.3 Truncated flow equations

The flow equation is nearly impossible to solve without a truncation to a reasonable subspace of the theory. The first simplifying assumption we make reduces much of the effort, while still being very general: Neglecting the evolution of the ghosts, with the ansatz

$$\Gamma_k\left[g,\overline{g},\xi,\overline{\xi}\right]=\Gamma_k\left[\overline{h}+\overline{g},0,0\right]+S_{\mathrm{gh}}\left[0,\xi,\overline{\xi};\overline{g}\right]+S_{\mathrm{gf}}\left[\overline{h};\overline{g}\right]. \tag{3.17}$$

The chosen ansatz ensures that mixed $h-C$ terms in equation (3.16) vanish, simplifying the derivative w.r.t the ghosts. One then obtains

$$\partial_t\Gamma_k=\mathrm{Tr}\left\{\frac{1}{2}\left(\Gamma_k^{(2)}\left[g,\overline{g}\right]+R_k^{\mathrm{grav}}\left[\overline{g}\right]\right)^{-1}\left(\partial_tR_k^{\mathrm{grav}}\left[\overline{g}\right]\right)-\left(-\kappa^{-1}\mathcal{M}\left[\overline{g},\overline{g}\right]+R_k^{\mathrm{gh}}\left[\overline{g}\right]\right)^{-1}\left(\partial_tR_k^{\mathrm{gh}}\left[\overline{g}\right]\right)\right\}. \tag{3.18}$$

This simplification is not yet sufficient for us to be able to perform computations. We needs to limit ourselves to a specific truncation. In order to extract the flow, we work with the Einstein-Hilbert truncation.

3.2 The Einstein-Hilbert truncation

3.2.1 The quadratic action

The simplest example of a truncation is the EH truncation,

$$\begin{aligned}\Gamma_k\left[g,\overline{g}\right] = 2\kappa^2 Z_{Nk}\int d^dx\sqrt{\overline{g}}\left(-R+2\overline{\Lambda}_k\right)\\ +\kappa^2 Z_{Nk}\int d^dx\sqrt{\overline{g}\overline{g}}^{\mu\nu}\mathcal{F}_\mu^{\alpha\beta}g_{\alpha\beta}\mathcal{F}_\nu^{\rho\sigma}g_{\rho\sigma},\end{aligned} \tag{3.19}$$

with the scale dependence of the action absorbed into the couplings [33],

$$\overline{\Lambda}\to\overline{\Lambda}_k,\quad \overline{G}\to G_k=\overline{G}Z_{N_k}^{-1}.$$

Z_{Nk} is the field strength renormalization, and the gauge-fixing function is chosen to be the De-Donder gauge [1],

$$\mathcal{F}_\mu^{\alpha\beta}h_{\alpha\beta}=\sqrt{2}\kappa\left(\overline{D}_\gamma h^\gamma{}_\mu-\frac{1}{2}\overline{D}_\mu h\right).$$

We will eventually set $g=\overline{g}$ to cancel the gauge fixing term, because $\overline{D}_\mu$ involves the background Christoffel symbol $\overline{\Gamma}$ and thus $\overline{D}_\mu\overline{g}_{\alpha\beta}=0$. We begin by obtaining Γ_k^{quad}[1, 34, 35]. Combined with the gauge fixing term, one finds

$$\Gamma_k^{\text{quad}}\left[\overline{h};\overline{g}\right]=Z_{N_k}\kappa^2\int d^dx\sqrt{\overline{g}}\overline{h}_{\mu\nu}\left[-K^{\mu\nu}{}_{\rho\sigma}\left(\overline{D}^2+2\overline{\Lambda}_k\right)+U^{\mu\nu}{}_{\rho\sigma}\right]\overline{h}^{\rho\sigma}, \tag{3.20}$$

with

$$K^{\mu\nu}{}_{\rho\sigma}=\frac{1}{4}\left[\delta^\mu_\rho\delta^\nu_\sigma+\delta^\mu_\sigma\delta^\nu_\rho-\overline{g}^{\mu\nu}\overline{g}_{\rho\sigma}\right], \tag{3.21}$$

and

$$\begin{aligned}U^{\mu\nu}{}_{\rho\sigma}=&K^{\mu\nu}{}_{\rho\sigma}\overline{R}+\frac{1}{2}\left[\overline{g}^{\mu\nu}\overline{R}_{\rho\sigma}+\overline{g}_{\rho\sigma}\overline{R}^{\mu\nu}\right]\\ &-\frac{1}{4}\left[\delta^\mu_\rho\overline{R}^\nu_\sigma+\delta^\nu_\rho\overline{R}^\mu_\sigma+\delta^\mu_\sigma\overline{R}^\nu_\rho+\delta^\nu_\sigma\overline{R}^\mu_\rho\right]-\frac{1}{2}\left[\overline{R}^\mu{}_\rho{}^\nu{}_\sigma+\overline{R}^\mu{}_\sigma{}^\nu{}_\rho\right].\end{aligned} \tag{3.22}$$

In the ghosts sector, the action is

$$S_{\text{gh}}\left[h,C,\overline{C};\overline{g}\right]=-\kappa^{-1}\int d^dx\sqrt{\overline{g}}\overline{C}_\mu\mathcal{M}\left[g,\overline{g}\right]^\mu{}_\nu C^\nu, \tag{3.23}$$

where

$$\mathcal{M}\left[g,\overline{g}\right]^{\mu}{}_{\nu}=\sqrt{2}\kappa\left(\overline{g}^{\mu\rho}\overline{g}^{\sigma\lambda}\overline{D}_{\lambda}\left(g_{\rho\nu}D_{\sigma}+g_{\sigma\nu}D_{\rho}\right)-\overline{g}^{\rho\sigma}\overline{g}^{\mu\lambda}\overline{D}_{\lambda}g_{\sigma\nu}D_{\rho}\right). \tag{3.24}$$

Implementing the ansatz (3.17),

$$\begin{aligned}\kappa^{-1}\mathcal{M}\left[\overline{g},\overline{g}\right]^{\mu}{}_{\nu}&=\sqrt{2}\left(\delta^{\mu}{}_{\nu}\overline{D}^{2}+\left[\overline{D}_{\nu},\overline{D}^{\mu}\right]\right)\\&=\sqrt{2}\left(\delta^{\mu}{}_{\nu}\overline{D}^{2}+\overline{R}^{\mu}{}_{\nu}\right).\end{aligned} \tag{3.25}$$

Having obtained the coefficient of the Laplacian in (3.20), we can now choose the form of the cutoffs. In order to suppress IR modes of the *background* covariant Laplacian, we choose

$$R_{k}^{\mathrm{grav}\,\mu\nu}{}_{\rho\sigma}\left(-\overline{D}^{2}\right)=Z_{N_{k}}K^{\mu\nu}{}_{\rho\sigma}R_{k}\left(-\overline{D}^{2}/k^{2}\right), \tag{3.26a}$$

$$R_{k}^{\mathrm{gh}}\left(-\overline{D}^{2}\right)^{\mu}{}_{\nu}=\delta^{\mu}{}_{\nu}R_{k}\left(-\overline{D}^{2}/k^{2}\right), \tag{3.26b}$$

where $R_{k}=k^{2}R_{k}^{(0)}\left(-\overline{D}^{2}/k^{2}\right)$ is the cutoff type and the renormalization of the ghosts had been neglected, i.e. $Z_{\mathrm{gh}}=1$. $R_{k}^{(0)}\left(-\overline{D}^{2}/k^{2}\right)$ is chosen in appendix C. The modified inverse graviton propagator is then

$$\mathbf{\Gamma}_{k}^{(2)}+\mathbf{R}_{k}=Z_{N_{k}}\mathbf{K}\left(P_{k}^{\mathrm{grav}}\left(-\overline{D}^{2}\right)-2\overline{\Lambda}_{k}+\mathbf{W}\right), \tag{3.27}$$

where $P_{k}^{\mathrm{grav}}=-\overline{D}^{2}+R_{k}^{\mathrm{grav}},\mathbf{W}=2U^{\mu\nu}{}_{\rho\sigma}-\left(\frac{d-4}{d-2}\right)\overline{g}_{\rho\sigma}\left(\overline{R}^{\mu\nu}-\frac{1}{2}\overline{R}\overline{g}^{\mu\nu}\right)$ as defined in appendix B. So long as $\mathbf{W}$ is linear in curvature, we can expand the propagator in powers of curvature,

$$\begin{aligned}\left(\mathbf{\Gamma}_{k}^{(2)}+\mathbf{R}_{k}\right)^{-1}&=\left(Z_{N_{k}}\mathbf{K}\left(P_{k}^{\mathrm{grav}}-2\overline{\Lambda}_{k}\right)\right)^{-1}\frac{1}{1+\frac{\mathbf{W}}{P_{k}^{\mathrm{grav}}-2\overline{\Lambda}_{k}}}\\&=\left(Z_{N_{k}}\mathbf{K}\left(P_{k}^{\mathrm{grav}}-2\overline{\Lambda}_{k}\right)\right)^{-1}\sum_{n=0}^{\infty}\left(-\frac{\mathbf{W}}{P_{k}^{\mathrm{grav}}-2\overline{\Lambda}_{k}}\right)^{n}\\&=\left(Z_{N_{k}}\mathbf{K}\left(P_{k}^{\mathrm{grav}}-2\overline{\Lambda}_{k}\right)\right)^{-1}\left(\mathbf{1}-\frac{\mathbf{W}}{P_{k}^{\mathrm{grav}}-2\overline{\Lambda}_{k}}+\mathcal{O}\left(R^{2}\right)\right).\end{aligned} \tag{3.28}$$

Similarly for the ghosts,

$$\left(-\mathcal{M}\left[\overline{g},\overline{g}\right]+R_k^{\mathrm{gh}}\left[\overline{g}\right]\right)^{-1}=\left(\overbrace{\delta^{\mu}{}_{\nu}\left(k^2R_k^{(0)}\left(-\overline{D}^2/k^2\right)-\overline{D}^2\right)}^{P_k^{\mathrm{gh}}}-\overline{R}^{\mu}{}_{\nu}\right)^{-1} \tag{3.29}$$
$$\equiv\left(\delta^{\mu}{}_{\rho}P_k^{\mathrm{gh}}\right)^{-1}\left(\delta^{\rho}{}_{\nu}+\frac{\overline{R}^{\rho}{}_{\nu}}{P_k^{\mathrm{gh}}}+\mathcal{O}\left(R^2\right)\right).$$

3.2.2 Trace expansion

We follow [34] and combine (3.28) with the heat-kernel expansion we discuss in appendix B. The r.h.s of (3.18) becomes

$$\begin{aligned}\mathrm{RHS}=&\frac{1}{2}\mathrm{Tr}\left\{\frac{\left(\eta+\partial_t\right)R_k\left(-\overline{D}^2/k^2\right)}{P_k^{\mathrm{grav}}-2\overline{\Lambda}_k}\left(\mathbf{1}-\frac{\mathbf{W}}{P_k^{\mathrm{grav}}-2\overline{\Lambda}_k}\right)\right\}\\&\text{-}\mathrm{Tr}\left\{\frac{\partial_tR_k\left(-\overline{D}^2/k^2\right)}{P_k^{\mathrm{gh}}}\left(\mathbf{1}+\frac{\overline{R}^{\rho}{}_{\nu}}{P_k^{\mathrm{gh}}}\right)\right\}+\mathcal{O}\left(R^2\right)\\&=\frac{1}{(4\pi)^{d/2}}\int d^dx\sqrt{\overline{g}}\left\{\frac{1}{2}Q_{\frac{d}{2}}\left(\frac{\left(\eta+\partial_t\right)R_k}{P_k^{\mathrm{grav}}-2\overline{\Lambda}_k}\right)\mathrm{tr}_{\mathrm{ST}}1-\frac{1}{2}Q_{\frac{d}{2}}\left(\frac{\left(\eta+\partial_t\right)R_k}{\left(P_k^{\mathrm{grav}}-2\overline{\Lambda}_k\right)^2}\right)\mathrm{tr}\mathbf{W}\right.\\&+\frac{1}{2}Q_{\frac{d}{2}-1}\left(\frac{\left(\eta+\partial_t\right)R_k}{P_k^{\mathrm{grav}}-2\overline{\Lambda}_k}\right)\frac{\overline{R}}{6}\mathrm{tr}_{\mathrm{ST}}1-Q_{\frac{d}{2}}\left(\frac{\partial_tR_k}{P_k^{\mathrm{gh}}}\right)\mathrm{tr}_{\mathrm{V}}1\\&\left.-Q_{\frac{d}{2}-1}\left(\frac{\partial_tR_k}{P_k^{\mathrm{gh}}}\right)\left(\frac{\overline{R}}{6}\mathrm{tr}_{\mathrm{V}}1\right)-Q_{\frac{d}{2}}\left(\frac{\partial_tR_k}{\left(P_k^{\mathrm{gh}}\right)^2}\right)\overline{R}+\mathcal{O}\left(R^2\right)\right\},\end{aligned} \tag{3.30}$$

where $\eta\equiv\partial_tZ_{N_k}/Z_{N_k}$ is the anomalous dimension associated with the invariant $\int d^dx\sqrt{\overline{g}}R$. The subscripts $(\mathrm{ST})\,,(\mathrm{V})$ imply the tracing is done over symmetric-tensor and vector degrees of freedom, respectively. In the second equality we used (B.2), only keeping first-order in curvature terms. We evaluate the traces,

$$\mathrm{tr}_{\mathrm{ST}}1=\frac{d\left(d+1\right)}{2}, \tag{3.31a}$$
$$\mathrm{tr}_{\mathrm{V}}1=d, \tag{3.31b}$$
$$\mathrm{tr}\mathbf{W}=\frac{d\left(d-1\right)}{2}\overline{R}. \tag{3.31c}$$

With the insertion of equations (3.31), (3.30) becomes

$$\begin{aligned}\text{RHS} =& \frac{1}{(4\pi)^{d/2}} \int d^d x \sqrt{\overline{g}} \left\{ \frac{d\,(d+1)}{4} Q_{\frac{d}{2}} \left(\frac{(\eta + \partial_t)\, R_k}{P_k^{\text{grav}} - 2\overline{\Lambda}_k} \right) - d Q_{\frac{d}{2}} \left(\frac{\partial_t R_k}{P_k^{\text{gh}}} \right) \right. \\ &+ \overline{R} \left[\frac{d\,(d+1)}{24} Q_{\frac{d}{2}-1} \left(\frac{(\eta + \partial_t)\, R_k}{P_k^{\text{grav}} - 2\overline{\Lambda}_k} \right) - \frac{d}{6} Q_{\frac{d}{2}-1} \left(\frac{\partial_t R_k}{P_k^{\text{gh}}} \right) \right. \\ &\left. - \frac{d\,(d-1)}{4} Q_{\frac{d}{2}} \left(\frac{(\eta + \partial_t)\, R_k}{\left(P_k^{\text{grav}} - 2\overline{\Lambda}_k\right)^2} \right) - Q_{\frac{d}{2}} \left(\frac{\partial_t R_k}{\left(P_k^{\text{gh}}\right)^2} \right) \right] \\ &\left. + \mathcal{O}\left(R^2\right) \right\}. \end{aligned} \tag{3.32}$$

On the l.h.s we take the derivative w.r.t $t = \ln k$ and set $g_{\mu\nu} = \overline{g}_{\mu\nu}$,

$$\partial_t \Gamma_k = 2\kappa^2 \int d^d x \sqrt{\overline{g}} \left(-\overline{R} \partial_t Z_{N_k} + 2\partial_t \left(Z_{N_k} \overline{\Lambda}_k \right) \right). \tag{3.33}$$

Combined with the r.h.s, one obtains the RG equation for Z_{N_k},

$$\begin{aligned}\partial_t Z_{N_k} =& -\frac{\overline{G}}{(4\pi)^{d/2-1}} \left[\frac{d\,(d+1)}{6} Q_{\frac{d}{2}-1} \left(\frac{(\eta + \partial_t)\, R_k}{P_k^{\text{grav}} - 2\overline{\Lambda}_k} \right) - \frac{2d}{3} Q_{\frac{d}{2}-1} \left(\frac{\partial_t R_k}{P_k^{\text{gh}}} \right) \right. \\ &\left. - d\,(d-1)\, Q_{\frac{d}{2}} \left(\frac{(\eta + \partial_t)\, R_k}{\left(P_k^{\text{grav}} - 2\overline{\Lambda}_k\right)^2} \right) - 4 Q_{\frac{d}{2}} \left(\frac{\partial_t R_k}{\left(P_k^{\text{gh}}\right)^2} \right) \right], \end{aligned} \tag{3.34}$$

and $Z_{N_k} \overline{\Lambda}_k$,

$$\partial_t \left(Z_{N_k} \overline{\Lambda}_k \right) = \frac{1}{2} \frac{\overline{G}}{(4\pi)^{d/2-1}} \left[d\,(d+1)\, Q_{\frac{d}{2}} \left(\frac{(\eta + \partial_t)\, R_k}{P_k^{\text{grav}} - 2\overline{\Lambda}_k} \right) - 4d Q_{\frac{d}{2}} \left(\frac{\partial_t R_k}{P_k^{\text{gh}}} \right) \right]. \tag{3.35}$$

3.2.3 Flow equations

Using the Φ-functionals defined in appendix C, we insert (C.3) into equations (3.34) and (3.35) and arrive at the flow equations

$$\eta = -\frac{g_k}{(4\pi)^{d/2-1}}\left[\eta\left(\frac{d\,(d+1)}{6}\tilde{\Phi}^1_{\frac{d}{2}-1}\left(-2\Lambda_k\right) - d\,(d-1)\,\tilde{\Phi}^2_{\frac{d}{2}}\left(-2\Lambda_k\right)\right)\right. \tag{3.36a}$$

$$\left. + \frac{d\,(d+1)}{3}\overline{\Phi}^1_{\frac{d}{2}-1}\left(-2\Lambda_k\right) - \frac{4d}{3}\overline{\Phi}^1_{\frac{d}{2}-1}\left(0\right) - 2d\,(d-1)\,\overline{\Phi}^2_{\frac{d}{2}}\left(-2\Lambda_k\right) - 8\overline{\Phi}^2_{\frac{d}{2}}\left(0\right)\right],$$

$$\partial_t\Lambda_k = -\left(2+\eta\right)\Lambda_k + \frac{1}{2}\frac{g_k}{(4\pi)^{d/2-1}}\left[d\,(d+1)\,\eta\tilde{\Phi}^1_{\frac{d}{2}}\left(-2\Lambda_k\right) + 2d\,(d+1)\,\overline{\Phi}^1_{\frac{d}{2}}\left(-2\Lambda_k\right) - 8d\overline{\Phi}^1_{\frac{d}{2}}\left(0\right)\right], \tag{3.36b}$$

where the dimensionless couplings

$$\Lambda_k \equiv k^{-2}\overline{\Lambda}_k, \tag{3.37}$$

and

$$g_k \equiv k^{d-2}G_k = Z_{N_k}^{-1}\overline{G}k^{d-2}, \tag{3.38}$$

have been used. From equations (3.36) we find that

$$\eta = -\frac{g_k B_1}{1+g_k B_2}, \tag{3.39}$$

with

$$B_1\left(\Lambda_k\right) = \frac{(4\pi)^{1-d/2}}{3}\left(d\,(d+1)\,\overline{\Phi}^1_{\frac{d}{2}-1}\left(-2\Lambda_k\right) - 4d\overline{\Phi}^1_{\frac{d}{2}-1}\left(0\right) - 6d\,(d-1)\,\overline{\Phi}^2_{\frac{d}{2}}\left(-2\Lambda_k\right) - 24\overline{\Phi}^2_{\frac{d}{2}}\left(0\right)\right), \tag{3.40a}$$

$$B_2\left(\Lambda_k\right) = \frac{(4\pi)^{1-d/2}}{6}\left(d\,(d+1)\,\tilde{\Phi}^1_{\frac{d}{2}-1}\left(-2\Lambda_k\right) - 6d\,(d-1)\,\tilde{\Phi}^2_{\frac{d}{2}}\left(-2\Lambda_k\right)\right). \tag{3.40b}$$

The β function for g_k is gotten by differentiating equation (3.38),

$$\beta_g\left(g,\Lambda\right) = \partial_t g_k = \left(-\eta + d - 2\right)g_k, \tag{3.41}$$

and when replacing η by (3.39), the resulting β functions are

$$\beta_g\left(g,\Lambda\right)=\frac{g_k^2 B_1\left(\Lambda_k\right)}{1+g_k B_2\left(\Lambda_k\right)}+\left(d-2\right)g_k, \tag{3.42}$$

and

$$\beta_\Lambda\left(g,\Lambda\right)=-\left(2+\eta\right)\Lambda_k+\frac{1}{2}\frac{g_k}{\left(4\pi\right)^{d/2-1}}\left[d\left(d+1\right)\eta\tilde{\Phi}^1_{\frac{d}{2}}\left(-2\Lambda_k\right)+2d\left(d+1\right)\overline{\Phi}^1_{\frac{d}{2}}\left(-2\Lambda_k\right)-8d\overline{\Phi}^1_{\frac{d}{2}}\left(0\right)\right]. \tag{3.43}$$

3.2.4 The RG flow of QEG in $d=4$

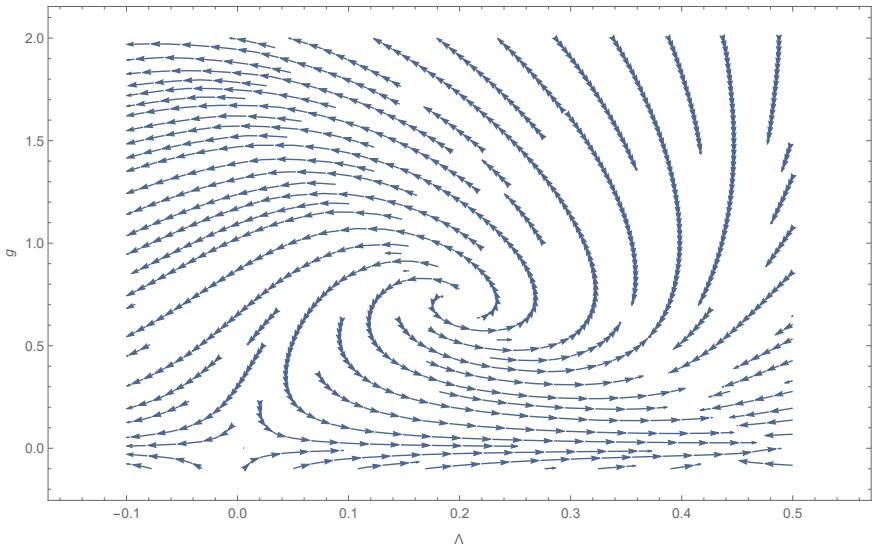

Figure 3.1: RG flow in the phase space of g_k, Λ_k in $d=4$.

The Gaussian and non-Gaussian fixed points (NGFP) for g_k, Λ_k are

$$g^*=0, \Lambda^*=0, \tag{3.44}$$

$$g^*=0.707, \Lambda^*=0.193, \tag{3.45}$$

with additional complex fixed points,

$$g^*=4.69\pm 1.33i, \Lambda^*=-0.078\pm 0.603i. \tag{3.46}$$

For a complete phase portrait with an explicitly marked limit cycle the reader

is referred to [6]. As argued in e.g. [1, 2, 33], there exists a NGFP in the flow profile such that at this point $g^*\Lambda^* = 0.136$, in agreement with the universal quantity found in [36]. Linearizing the flow around the fixed points such that

$$\beta_i = \sum_i B_{ij} \left(j\left(k\right) - j^* \right), \tag{3.47}$$

where $i, j = g, \Lambda$, and

$$B_{ij} \equiv \partial_j \beta_i \left(i^* \right), \tag{3.48}$$

one obtains from (3.47) the relation

$$\partial_t u_i \left(k\right) = \sum_j \partial_j \beta_i \left(u^*\right) \left(u_j \left(k\right) - u_j^* \right), \tag{3.49}$$

where $u_i\left(k\right), u_i^*$ are the couplings and their fixed points, respectively. The general solution to equation (3.49) is [2]

$$u_i \left(k\right) = u_i^* + \sum_I C_I V_i^I \left(\frac{k_0}{k} \right)^{\theta_I}, \tag{3.50}$$

with integration constants C_I and some reference scale k_0. V_i^I are the right eigenvectors of $\mathbf{B}$, with eigenvalues $-\theta_I$, and because $\mathbf{B}$ is not necessarily symmetric, they can be both real and complex. Equation (3.50) reflects the leading-order scaling of the flow near the fixed points, with θ_I referred to as "critical exponents" since, in second-order phase transitions, they are linear in the critical exponents [37]. Near the NGFP (3.45),

$$\theta_\pm = 1.47 \pm 3.04i, \tag{3.51}$$

indicating the NGFP is UV attractive ($\mathfrak{Re}\theta > 0$). The complex critical exponents reveal that trajectories emanating from the NGFP are, to leading order, spiral trajectories which have the DSI form of 2.1.1. From figure 3.1 and equation (3.50) one concludes that in the vicinity of the NGFP the couplings behave like self-similar fractals. The critical exponents of the complex flow solutions are

$$-3.07 - 4.26i, -2.29 - 0.91i,$$

both with a negative real part, indicating that the limit cycle is UV repulsive and emanates spiral trajectories as well.

To understand the meaning of a limit cycle in the flow of a quantum-gravitational theory, we recall the Callan-Symanzic equation,

$$\left(\partial_{\ln k} + \beta\left(g_k\right)\partial_{g_k} + \beta\left(\Lambda_k\right)\partial_{\Lambda_k} - n\eta\right)\mathcal{G}^{(n)}\left(x; g_k, \Lambda_k, k\right) = 0, \tag{3.52}$$

where $\mathcal{G}^{(n)}\left(x; g_k, \Lambda_k, k\right)$ is the n-point correlation function of the gravitational field. When $x \to e^{\lambda}x$ it follows that

$$\left(-\partial_{\lambda} + \beta\left(g_k\right)\partial_{g_k} + \beta\left(\Lambda_k\right)\partial_{\Lambda_k} - n\eta\right)\mathcal{G}^{(n)}\left(e^{\lambda}x; g_k, \Lambda_k, k\right) = 0. \tag{3.53}$$

This scaling relation is formally solved by integration [38] to give

$$\begin{aligned}\mathcal{G}^{(n)}\left(e^{\lambda}x; g_k\left(0\right), \Lambda_k\left(0\right), k\right) = &\exp\left[n\int_{g_k(0)}^{g_k(\lambda)} dg_k \frac{\eta\left(g_k, \Lambda_k\left(g_k\right)\right)}{\beta_g\left(g_k, \Lambda_k\left(g_k\right)\right)}\right] \\ &\times \mathcal{G}^{(n)}\left(x, g_k\left(\lambda\right), \Lambda_k\left(\lambda\right)\right).\end{aligned} \tag{3.54}$$

When g_k and Λ_k have a limit cycle with period T, they satisfy

$$g_k\left(0\right) = g_k\left(T\right), \Lambda_k\left(0\right) = \Lambda_k\left(T\right). \tag{3.55}$$

Replacing T for λ in equation (3.54) results in the n-point function repeating itself periodically,

$$\mathcal{G}^{(n)}\left(e^{T}x; g_k, \Lambda_k, k\right) = \mathcal{G}^{(n)}\left(x, g_k, \Lambda_k\right). \tag{3.56}$$

Since this scaling symmetry only holds for $\lambda = e^{T}$, we conclude that the correlation functions of QEG are DSI functions. In particular, on the limit cycle the spacetime is a fractal,

$$\left\langle g_{\mu\nu}\left(e^{T}x\right)\right\rangle = \left\langle g_{\mu\nu}\left(x\right)\right\rangle. \tag{3.57}$$

3.3 The QEG flow as a substitution tiling

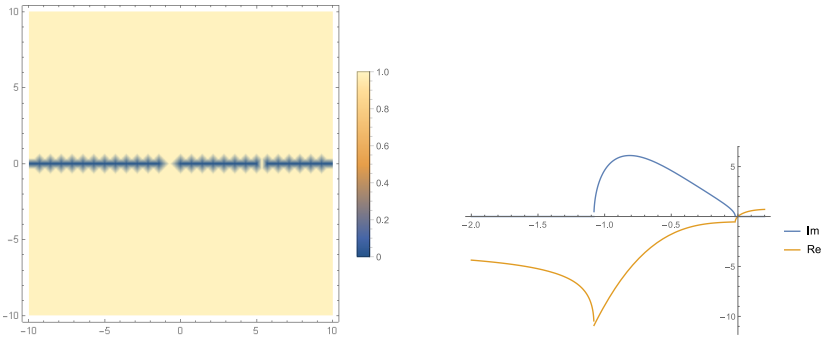

Figure 3.2: Left: $\mathfrak{Im} g_k(\Lambda)$ as a function of $x + iy \equiv \Lambda$. Right: $\mathfrak{Im} g_k(\mathfrak{Re}\Lambda), \mathfrak{Re} g_k(\mathfrak{Re}\Lambda)$.

We consider $\beta_\Lambda \approx 0$, a valid assumption near a stationary point of the flow. A vanishing flow in Λ results in a quadratic equation for g_k,

$$0 = -g_k^2 + 12\pi g_k \frac{-3 + \Lambda\left(3 + 2\Lambda + 56\Lambda^2\right)}{107 - 20\Lambda} + 144\pi^2 \frac{\Lambda\left(1 - 2\Lambda\right)^2}{107 - 20\Lambda}.$$

If we assume g_k is also close to its fixed points, we can use $g_k^2 \approx g_{k+1} g_k$ and obtain

$$g_{k+1} g_k = g_k 12\pi \frac{-3 + \Lambda\left(3 + 2\Lambda + 56\Lambda^2\right)}{107 - 20\Lambda} + 144\pi^2 \frac{\Lambda\left(1 - 2\Lambda\right)^2}{107 - 20\Lambda}. \tag{3.58}$$

Note that the form of (3.58) resembles that of the Efimov mapping, with the QEG occurrence matrix being

$$M_{QEG} = \begin{pmatrix} 12\pi \frac{-3+\Lambda\left(3+2\Lambda+56\Lambda^2\right)}{107-20\Lambda} & 144\pi^2 \frac{\Lambda(1-2\Lambda)^2}{107-20\Lambda} \\ 1 & 0 \end{pmatrix}. \tag{3.59}$$

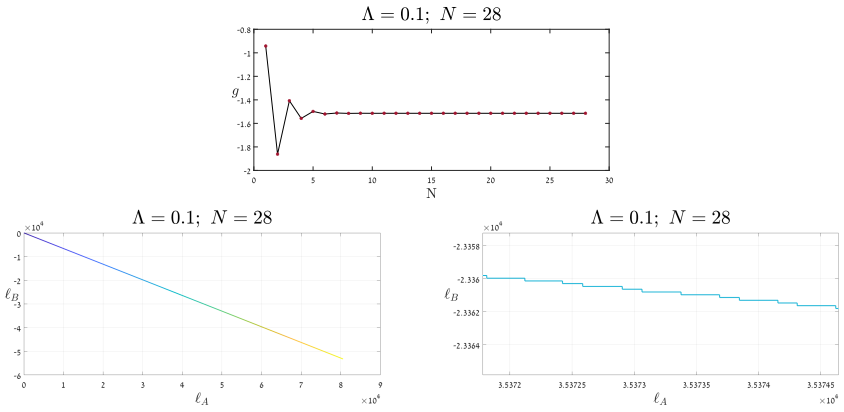

Figure 3.3: At $\Lambda = 0.1$, g_k is periodic.

We wish to interpret the eigenvectors of M_{QEG} as the fixed points like we did for Efimov physics. Unfortunately, their dependence on Λ is much more complicated.

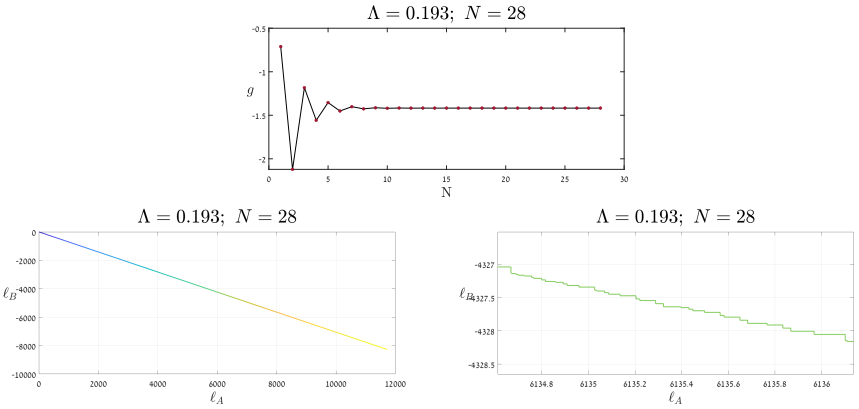

Figure 3.4: At $\Lambda = 0.193$, g_k is periodic.

It is illuminating, however, to replace Λ by the fixed points found in section 3.2.4, as it turns out that the ratio of entries of eigenvectors indeed agrees with the fixed points of g_k. Figure 3.2 illustrates the dependence of $\mathfrak{Im} g_k(\Lambda)$ and $g_k(\Lambda)$ on Λ.

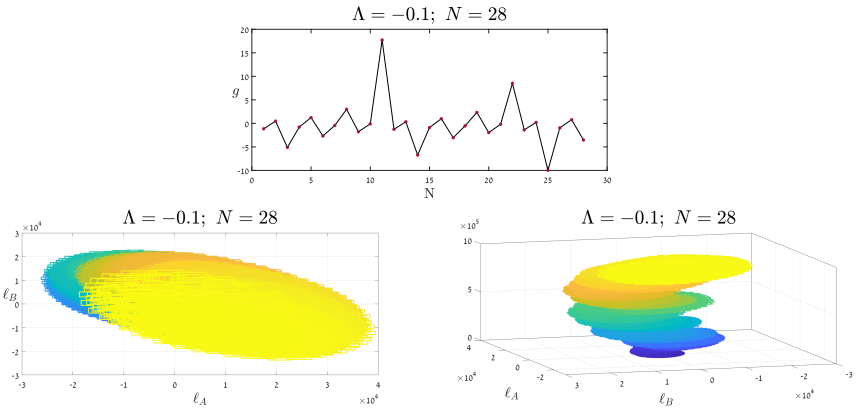

Figure 3.5: At $\Lambda = -0.1$, g_k is quasi-periodic.

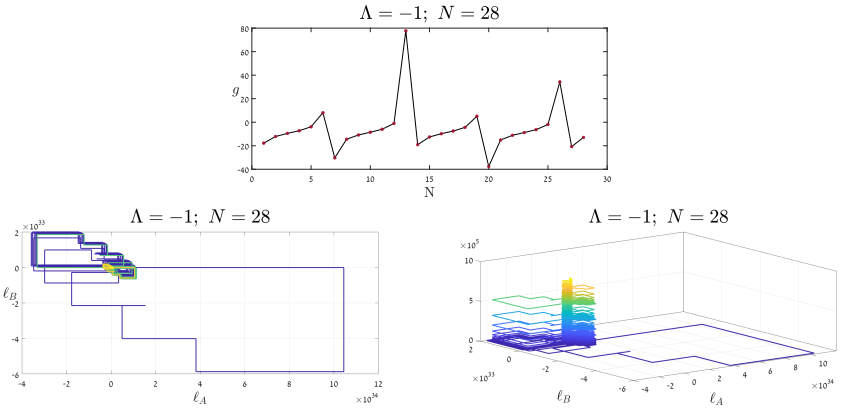

Figure 3.6: At $\Lambda = -1$, g_k is aperiodic.

It is evident in the plotted sequences for different values of Λ in figures 3.3-3.8, alongside respective values of g, that various different scaling behaviors occur. We recover the same phase transition of periodic to fractal tilings, corresponding to the proximity of Λ to its fixed points or to its limit cycle, respectively.

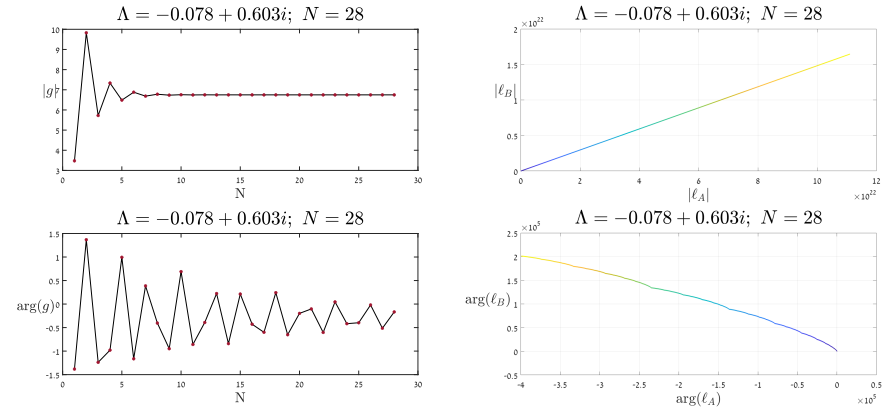

Figure 3.7: At $\Lambda = -0.078 \pm 0.603i$, $|g_k|$ is periodic, but its argument $\arg(g_k)$ is discretely self similar.

For $\Lambda = -0.078 \pm 0.603i$, the point of the limit cycle, we find a fractal tiling in the argument of the complex functions that make g, ℓ_A, ℓ_B. We present in figure 3.8 the subsequent zoom-ins into this fractal, which unvail its discrete self-similarity explicitly.

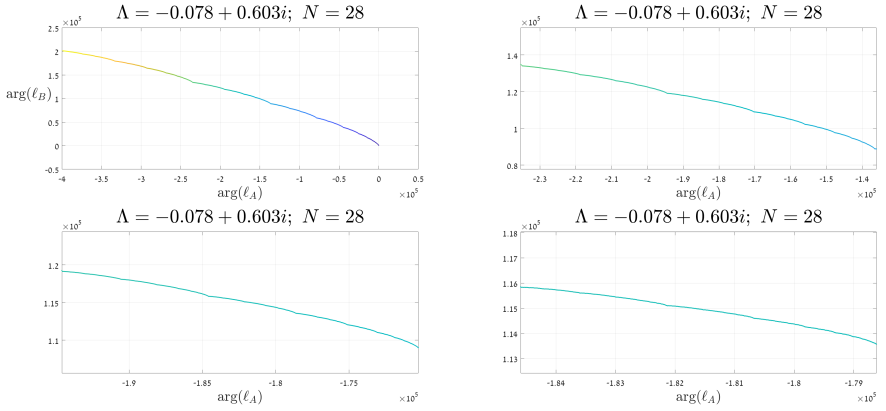

Figure 3.8: For $\Lambda = -0.078 \pm 0.603i$, close-ups of each segment of this fractal look precisely like the original shape.

4 Conclusions

We have studied a mapping from RG flows to substitution processes and tested it on two seemingly unrelated subjects - Efimov physics and the Einstein-Hilbert truncation of QEG. We obtained tilings for each theory, in both cases observing the same phase transition from CSI to DSI tilings. The occurrence matrix for Efimov had ξ as a control parameter in its phase transition, and a critical value identical to that of the transition of its flow from real to complex fixed points, $\xi = \xi_c$. In QEG we were not able to produce a control parameter and a critical value due to the complex nature of the Einstein-Hilbert flow. We obtained the phase transition by replacing different values of the cosmological constant Λ into the occurrence matrix, and found correlation between fractal tilings and limit cycles in the flow. In order to obtain this fractal tiling one must supplement known values of fixed points into the matrix, which was not necessary in the Efimov case. Furthermore, the mapping predicts the fixed points of a quadratic flow such as Efimov, but unable to achieve the same for QEG. Because the Einstein-Hilbert flow can only be solved numerically, other truncations should be considered and tested with our mapping. Doing so would confirm the correlation of fractal tilings with limit cycle solutions (or their absence!) even in cases with no analytical solution to the flow, and strengthen our claim the QEG belongs to Efimov physics.

The conclusion that limit cycles in the RG flow of a quantum gravity theory translate to fractal tilings, begs one to wonder whether some sort of substitution process could be the underlying structure of our spacetime. There had recently been a surprising theory by Stephen Wolfram suggesting this very conclusion [39]. Another quantum theory of geometry reminiscent of this description is CDT. Although we did not examine it in this work, it is by construction a very interesting theory to approach from a substitution perspective: it uses simplices and matching rules as the building blocks of spacetime [40]. It might be that the mystery surrounding the interior of black holes and physics at the Planck length, could resolve in a universe that evolves as a substitution process.

Appendix

A Wetterich equation

A.0.0.1 An exact evolution of the effective action We follow the proof [41] for a set of real scalar fields $\{\varphi^a\}_{a=1}^N$, however one can easily generalize it to non-Abelian, Grassmann and vector fields. For an action $S[\varphi]$, the generating functional $W[J]$ is gotten by adding an appropriate source term,

$$W[J] = \ln \int \mathcal{D}\varphi e^{-S(\varphi)+J\cdot\varphi}, \tag{A.1}$$

with the convention that $J\cdot\varphi \equiv \int d^d y J(y)\varphi(y)$. Taking the Legendre transform of (A.1) gives the effective action

$$\Gamma[\phi] \equiv J\cdot\phi - W[J], \tag{A.2}$$

where $\phi = \langle\varphi\rangle = \delta W/\delta J$ is the classical (expectation) value of the field. We modify $W[J], \Gamma[\phi]$ to depend on the momentum scale k. IR degrees of freedom are suppressed up to this scale, to decouple the slow modes $p^2 \ll k^2$ from the rest and leave the fast modes unaffected, to be integrated out. This modification is introduced by adding a scale dependent "mass term" to the action,

$$\Delta S_k[\varphi] \equiv \frac{1}{2}\int \frac{d^d p}{(2\pi)^d} R_k(p)\varphi_a^*(p)\varphi^a(p), \tag{A.3}$$

where we've used $\varphi_a^*(p) = \varphi_a(-p)$ for real fields. $R_k(p)$ is a weight function, or "mass" term, which satisfies the following conditions:

- It recovers the 1PI generating functional $\Gamma[\varphi]$ in the IR limit,

$$\lim_{k^2/p^2\to 0} R_k(p) = 0, \Gamma(k=0) = \Gamma.$$

- It recovers the bare microscopic action S in the UV limit,

$$\lim_{k^2\to\infty} R_k(p) = \infty, \Gamma(k\to\infty) = S.$$

- It only weighs down modes slower than the probing scale k,

$$R_k\left(p^2 \ll k^2\right) > 0, R_k\left(p^2 \gg k^2\right) = 0.$$

The objective of R_k is to suppress the low modes $p^2 \ll k^2$, forcing this mass term to be e.g. $\propto k^2$ for kinetic terms of the form $-\partial^2$, $R_k\left(p^2\right) \propto Z_k k^2$ for renormalized kinetic terms such as $Z_k \left(\partial\phi\right)^2$, etc.

This scale dependence results in an **average** effective action $\Gamma_k\left[\varphi\right]$, with averaging taken over volumes $\sim k^{-d}$ (the coarse-graining or mass scale). The resulting action is

$$S_k = S - \int \frac{d^d p}{\left(2\pi\right)^d} J_a^* \left(p\right) \varphi^a \left(p\right) + \Delta S_k. \tag{A.4}$$

Equipped with scale dependence and initial conditions, it is natural to look for a flow equation of Γ_k. We define $\tilde{\Gamma}_k$,the Legendre transform of W_k,

$$\tilde{\Gamma}_k\left[\phi_k\right] = \int \frac{d^d p}{\left(2\pi\right)^d} J_a^* \left(p\right) \cdot \phi_k^a \left(p\right) - W_k\left[J\right], \tag{A.5}$$

such that

$$\frac{\partial \tilde{\Gamma}_k}{\partial \phi_k^a \left(p\right)} = J_a^* \left(p\right). \tag{A.6}$$

We also derive the connected two-point function through

$$\begin{aligned} \left(G_k\right)_b^a \left(p, p'\right) &= \frac{\delta^2 W_k}{\delta J_a^* \left(p\right) \delta J^b \left(p'\right)} \\ &= \frac{\partial \phi_k^a \left(p\right)}{\partial J^b \left(p'\right)} \\ &= \left\langle \varphi^a \left(p\right) \varphi_b^* \left(p'\right) \right\rangle - \phi_k^a \left(p\right) \phi_{bk}^* \left(p'\right). \end{aligned} \tag{A.7}$$

Note that

$$\frac{\delta^2 \tilde{\Gamma}_k}{\delta \phi_{bk}^* \left(p'\right) \delta \phi_k^a \left(p\right)} = \frac{\partial J^b \left(p\right)}{\partial \phi_k^a \left(p'\right)}, \tag{A.8}$$

so $\tilde{\Gamma}_k$ and W_k satisfy the identity

$$\int \frac{d^d p'}{\left(2\pi\right)^d} \left(G_k\right)_b^a \left(p, p'\right) \frac{\delta^2 \tilde{\Gamma}_k}{\delta \phi_{bk}^* \left(p'\right) \delta \phi_k^c \left(p''\right)} = \delta_{p,p''} \delta_c^a. \tag{A.9}$$

To obtain the dependence of $\tilde{\Gamma}_k$ on k, we fix φ_k and take the derivative w.r.t $t = \ln k$,

$$\partial_t \tilde{\Gamma}_k \big|_{\varphi_k} = -\left.\partial_t W_k\right|_J = \partial_t \left\langle \Delta S_k \right\rangle = \frac{1}{2} \int \frac{d^d p}{\left(2\pi\right)^d} \partial_t R_k \left(p\right) \left\langle \varphi_a^* \left(p\right) \varphi^a \left(p\right) \right\rangle, \tag{A.10}$$

and thus

$$\partial_t \tilde{\Gamma}_k\big|_{\varphi_k} = \frac{1}{2}\int \frac{d^d p}{(2\pi)^d} \partial_t R_k(p) \left[(G_k)^a_a(p,p) + \phi^a_k(p)\, \phi^*_{ak}(p) \right]. \tag{A.11}$$

We now redefine

$$\Gamma_k = \tilde{\Gamma}_k - \frac{1}{2}\int \frac{d^d p}{(2\pi)^d} R_k(p)\, \phi^*_{ka}(p)\, \phi^a_k(p), \tag{A.12}$$

and obtain the flow of Γ_k,

$$\begin{aligned} \partial_t \Gamma_k|_{\varphi_k} &= \frac{1}{2}\int \frac{d^d p}{(2\pi)^d} \partial_t R_k(p)\, (G_k)^a_a(p,p) \\ &\equiv \frac{1}{2}\mathrm{Tr}\left(G_k \partial_t R_k\right), \end{aligned} \tag{A.13}$$

where the trace sums over all indices and momenta. As a final step we use the identity (A.9) to obtain

$$\begin{aligned} G_k &= \left(\frac{\partial^2 \tilde{\Gamma}_k}{\partial \phi^*_{ak} \partial \phi^a_k} \right)^{-1} \\ &= \left(\frac{\partial^2 \Gamma_k}{\partial \phi^*_{ak} \partial \phi^a_k} + R_k \right)^{-1}. \end{aligned} \tag{A.14}$$

The *exact* evolution equation for the effective action, commonly referred to as the Wetterich equation, then follows:

$$\partial_t \Gamma_k = \frac{1}{2}\mathrm{Tr}\left(\frac{\partial_t R_k}{\Gamma^{(2)}_k[\phi] + R_k} \right). \tag{A.15}$$

Note that in position space,

$$\Delta S_k[\varphi] = \frac{1}{2}\int d^d x \varphi(x)\, R_k\left(-\partial^2\right) \varphi(x),$$

so the trace in equation (A.15) involves spacetime integration.

B Heat kernel technique

The trace involves the inverse propagator

$$\frac{\delta^2 \Gamma_k}{\delta \bar{h} \delta \bar{h}},$$

which we will consider for $\overline{h}=0$, since it is quadratic in $\overline{h}$ and we want to cancel contributions from the gauge-fixing term. One needs only keep quadratic terms in Γ_k, which suggests the expansion

$$\Gamma_k\left[g,\overline{g}\right]=\Gamma_k\left[\overline{g},\overline{g}\right]+\mathcal{O}\left(\overline{h}\right)+\Gamma_k^{\mathrm{quad}}\left[\overline{h};\overline{g}\right]+\mathcal{O}\left(\overline{h}^3\right),$$

where

$$\Gamma_k^{\mathrm{quad}}\left[\overline{h};\overline{g}\right]=\frac{1}{2}\int d^dx\sqrt{\overline{g}}\overline{h}\frac{\delta^2\Gamma_k}{\delta\overline{h}\delta\overline{h}}\overline{h}.$$

The appropriate choice for R^{grav}, in order to suppress Γ_k^{quad}, is discussed in section 3.2.1. It must combine with the kinetic term into the form $-\overline{D}^2+k^2$ times some function or constant which are independent of the Laplacian. Both the quadratic contribution to the effective action and the suppression term R are functionals of the covariant Laplacian $-\overline{D}^2$. In order to evaluate the traces on the r.h.s of (3.18), we use the heat-kernal expansion of a Laplace-type operator,

$$\begin{aligned}\mathrm{Tr}W\left(\Delta\right)=\frac{1}{\left(4\pi\right)^{d/2}}\Big\{&Q_{\frac{d}{2}}\left(W\right)B_0\left(\Delta\right)+Q_{\frac{d}{2}-1}\left(W\right)B_2\left(\Delta\right)+\ldots\\&+Q_0\left(W\right)B_d\left(\Delta\right)+Q_{-1}\left(W\right)B_{d+2}\left(\Delta\right)+\ldots\Big\},\end{aligned}\tag{B.1}$$

where

$$\begin{aligned}Q_n\left[W\right]&=\frac{1}{\Gamma\left(n\right)}\int_0^\infty dzz^{n-1}W\left(z\right),\quad n>0,\\Q_0\left[W\right]&=W\left(0\right),\\Q_{-m}\left[W\right]&=\left(-1\right)^mW^{(m)}\left(0\right),\ m\in\mathbb{N},\end{aligned}$$

and $B_n=\int d^dx\sqrt{\overline{g}}\mathbf{b}_n$ are the known coefficients of the heat-trace asymptotic expansion when $s\to 0$. $\mathbf{b}_n$ are linear combinations of curvature tensors and their covariant derivatives, containing $2n$ derivatives of the metric. We then define

$$P_k\left(\Delta\right)\equiv-\overline{D}^2+R_k\left(\Delta\right),$$

where $\mathbf{R}_k=\kappa^2\mathbf{K}R_k$ is chosen, as discussed in (3.26a). Then, the trace reduces to

$$\mathrm{Tr}\frac{\partial_tR_k\left(\Delta\right)}{P_k\left(\Delta\right)+q\mathbf{1}+\mathbf{W}}=\frac{1}{\left(4\pi\right)^{d/2}}\sum_{n=0}^\infty Q_{\frac{d}{2}-n}\left(\frac{\partial_tR_k}{P_k+q\mathbf{1}}\right)\int d^dx\sqrt{\overline{g}}\mathbf{b}_{2n}\left(-\nabla^2+\mathbf{W}\right).\tag{B.2}$$

In section 3.2.1 we find a quadratic action of the form $\mathbf{\Gamma}_k^{(2)} = \kappa^2 Z\mathbf{K}\left(-\overline{D}^2 + q\mathbf{1} + \mathbf{K}^{-1}\mathbf{U}\right) \equiv \kappa^2\mathbf{K}\left(-\overline{D}^2 + q\mathbf{1} + \mathbf{W}\right)$, with $\left[\mathbf{W}, \overline{D}^2\right] = 0$. The only relevant heat-trace coefficients are then given by [34]

$$\begin{aligned}\mathbf{b}_0 &= \mathrm{tr}\mathbf{1},\\ \mathbf{b}_2 &= \frac{\overline{R}}{6}\mathrm{tr}\mathbf{1} - \mathrm{tr}\mathbf{W}.\end{aligned}$$

Higher order coefficients are useful in other truncations not discuss in this work.

C Q-functionals

The formulated RG equations of the Einstein-Hilbert truncation contain some undetermined forms, which can be written as linear combinations of the following functionals,

$$\Phi_n^p(w) \equiv \frac{1}{\Gamma(n)}\int_0^\infty dz z^{n-1}\frac{zR_k^{(0)\prime}(z)}{\left[z + R_k^{(0)}(z) + w\right]^p}, \tag{C.1a}$$

$$\tilde{\Phi}_n^p(w) \equiv \frac{1}{\Gamma(n)}\int_0^\infty dz z^{n-1}\frac{R_k^{(0)}(z)}{\left[z + R_k^{(0)}(z) + w\right]^p}, \tag{C.1b}$$

so that the Q-functionals for $n > 0$ [42] are

$$Q_n\left(\frac{(\eta + \partial_t)R_k}{\left(P_k^{\mathrm{grav}} - 2\overline{\Lambda}_k\right)^p}\right) = k^{2(n-p+1)}\left[(\eta+2)\tilde{\Phi}_n^p\left(-2\overline{\Lambda}_k/k^2\right) - 2\Phi_n^p\left(-2\overline{\Lambda}_k/k^2\right)\right], \tag{C.2a}$$

$$Q_n\left(\frac{\partial_t R_k}{\left(P_k^{\mathrm{gh}}\right)^p}\right) = 2k^{2(n-p+1)}\left[\tilde{\Phi}_n^p(0) - \Phi_n^p(0)\right]. \tag{C.2b}$$

To be able to analytically solve for Φ, we choose the optimized cutoff function [43, 44]

$$R_k\left(z/k^2\right) = \left(k^2 - z\right)\Theta\left(k^2 - z\right),$$

for which

$$\Phi_n^p(w) \equiv -\frac{1}{(n+1)\,\Gamma(n)}\frac{1}{(1+w)^p}, \tag{C.3a}$$

$$\tilde{\Phi}_n^p(w) = \frac{1}{\Gamma(n+2)}\frac{1}{(1+w)^p}. \tag{C.3b}$$

We will also find it convenient to define

$$\overline{\Phi}_n^p(w) \equiv \tilde{\Phi}_n^p(w) - \Phi_n^p(w) = \frac{1}{\Gamma(n+1)}\frac{1}{(1+w)^p}. \tag{C.4}$$

References

[1] M. Reuter, Phys. Rev. D **57**, 971 (1998).

[2] M. Reuter and F. Saueressig, New Journal of Physics **14**, 055022 (2012).

[3] J. Ambjørn, J. Jurkiewicz, and R. Loll, Physical Review Letters **95**, 171301 (2005).

[4] G. Calcagni, Physical Review Letters **104**, 251301 (2010).

[5] L. Modesto, arXiv preprint arXiv:0812.2214 (2008).

[6] D. Litim and A. Satz, arXiv preprint arXiv:1205.4218 (2012).

[7] S. D. Głazek and K. G. Wilson, Physical Review Letters **89**, 230401 (2002).

[8] E. Braaten and H. Hammer, in *17th International IUPAP Conference on Few-Body Problems in Physics* (2003).

[9] E. Braaten and D. Phillips, Phys. Rev. A **70**, 052111 (2004).

[10] R. M. May, Science **177**, 900 (1972).

[11] J. E. Stone, X. L. Aubert, H. Maass, A. J. Phillips, M. Magee, M. E. Howard, S. W. Lockley, S. M. Rajaratnam, and T. L. Sletten, Scientific reports **9**, 1 (2019).

[12] D. Gitelman, *"Physical properties of self-similar systems-applications to fractals and quasiperiodic tilings*, Ph.D. thesis, Technion (2016).

[13] V. Efimov, Physics Letters B **33**, 563 (1970).

[14] O. Ovdat, J. Mao, Y. Jiang, E. Andrei, and E. Akkermans, Nature Communications **8**, 1 (2017).

[15] E. B. Kolomeisky and J. P. Straley, Phys. Rev. B **46**, 12664 (1992).

[16] H.-W. Hammer and L. Platter, Annual Review of Nuclear and Particle Science **60**, 207 (2010).

[17] P. Naidon and S. Endo, Reports on Progress in Physics **80**, 056001 (2017).

[18] H.-W. Hammer and L. Platter, Ann. Rev. Nucl. Part. Sci. **60**, 207 (2010).

[19] J. Johansen, B. DeSalvo, K. Patel, and C. Chin, Nature Physics **13**, 731 (2017).

[20] H.-W. Hammer and L. Platter, Philosophical Transactions of the Royal Society A: Mathematical, Physical and Engineering Sciences **369**, 2679 (2011).

[21] E. Mueller and T. L. Ho, cond-mat / 0403283 (2004).

[22] H.-W. Hammer and B. G. Swingle, Annals of Physics **321**, 306 (2006).

[23] S. R. Beane, P. F. Bedaque, L. Childress, A. Kryjevski, J. McGuire, and U. van Kolck, Phys. Rev. A **64**, 042103 (2001).

[24] J.-M. Luck, P. Moussa, and M. Waldschmidt, eds., *Number Theory and Physics* (Springer Berlin Heidelberg, 1990).

[25] C. Goodman-Strauss, Annals of Mathematics **147**, 181 (1998).

[26] J. Feder, *Fractals, pp. 10-25*, Physics of Solids and Liquids (Springer US, 2013).

[27] G. Edgar, *Measure, Topology, and Fractal Geometry, pp. 1-13*, Undergraduate Texts in Mathematics (Springer New York, 2007).

[28] C. Godrèche and J. M. Luck, Phys. Rev. B **45**, 176 (1992).

[29] J.-M. Dumont and A. Thomas, Theoretical Computer Science **65**, 153 (1989).

[30] V. Efimov, Sov. J. Nucl. Phys **12**, 101 (1971).

[31] D. B. Kaplan, J.-W. Lee, D. T. Son, and M. A. Stephanov, Phys. Rev. D **80**, 125005 (2009).

[32] O. Ovdat and E. Akkermans, "The breaking of continuous scale invariance to discrete scale invariance: a universal quantum phase transition," (2019), arXiv:1909.05505 [cond-mat.mes-hall] .

[33] O. Lauscher and M. Reuter, Phys. Rev. D **65**, 025013 (2001).

[34] A. Codello, R. Percacci, and C. Rahmede, Annals of Physics **324**, 414 (2009).

[35] R. Percacci, *An Introduction to Covariant Quantum Gravity and Asymptotic Safety*, 100 Years of General Relativity, Vol. 3 (World Scientific, 2017).

[36] M. Reuter and F. Saueressig, Physical Review D **65**, 065016 (2002).

[37] J. Berges, N. Tetradis, and C. Wetterich, Physics Reports **363**, 223 (2002), renormalization group theory in the new millennium. IV.

[38] A. LeClair and G. Sierra, Journal of Statistical Mechanics: Theory and Experiment **2004**, P08004 (2004).

[39] J. Gorard, "Some relativistic and gravitational properties of the wolfram model," (2020), arXiv:2004.14810 [cs.DM] .

[40] J. Ambjorn, J. Gizbert-Studnicki, A. Gorlich, J. Jurkiewicz, and R. Loll, Frontiers in Physics **8**, 247 (2020).

[41] C. Wetterich, Physics Letters B **301**, 90 (1993).

[42] D. Benedetti, K. Groh, P. F. Machado, and F. Saueressig, JHEP **06**, 079 (2011).

[43] D. F. Litim, Phys. Rev. D **64**, 105007 (2001).

[44] D. F. Litim, Physical Review Letters **92**, 201301 (2004).

המרחב-זמן ליד אורך פלאנק כריצוף א-מחזורי

חיבור מחקר
לשם מילוי חלקי של הדרישות לקבלת תואר מגיסטר למדעים בפיסיקה

תום שינדלמן

הוגש לסנט הטכניון - מכון טכנולוגי לישראל

תשרי תשפ"א, חיפה, ספטמבר 2020

המחקר נעשה בהנחיית פרופ. אריק אקרמן בפקולטה לפיסיקה

אני מודה לטכניון על התמיכה הכספית הנדיבה בהשתלמותי

תקציר מורחב:

תורת היחסות הכללית ותורת הקוונטים מהוות שני תחומים מוצלחים כאשר הן נבחנות לחוד, אך טרם נמצאה התורה שתאחד אותן הנקראת "כבידה קוונטית" ,אחד התחומים הפתוחים הדומיננטיים ביותר בפיזיקה. כיום קיימות מגוון תיאוריות של כבידה קוונטית המנסות ליישב את הסתירה בין יחסות לקוונטים, למשל תורת המיתרים הידועה. במסגרת תורת השדות הקוונטית, בשנת 1996 הצליח מרטין רויטר לקבל משוואה המתארת את זרימת חבורת הרנורמליזציה עבור כבידה ומצא עבור תורה זו נקודת שבת שאינה טריוויאלית באנרגיות גבוהות. תורתו של רויטר קרויה "כבידת איינשטיין קוונטית", והיא מהווה תורה אפקטיבית (ממוצעת) במסגרתה ניתן למצוא את זרימת חבורת הרנורמליזציה עבור כבידה במדויק .

תורתו של רויטר היא אחת מיני רבות שמנסות להסביר את המרחב-זמן באנרגיות גבוהות (או לחילופין, בסקאלות אורך קצרות). למרות השוני הרב בין הניסוחים של תאוריות אלו, ישנה תכונה שמאפיינת את המרחב-זמן של כבידת איינשטיין הקוונטית שחוזרת על עצמה בשלל תיאוריות נוספות - בקרבת אורך פלאנק, הפתרון למרחב-זמן הוא פרקטל. מרחב-זמן זה הוצע כפתרון של תיאורית שדות סטטיסטית עבור כבידה, של לולאות כבידה קוונטית ועוד. בכבידת איינשטיין הקוונטית, מרחב-זמן זה נובע מפתרון מיוחד למשוואות חבורת הרנורמליזציה: מחזורי גבול. פתרונות אלו מחזוריים ומאופיינים בסימטריה בדידה לשינוי הסקאלה, בשונה מנקודות שבת רגילות שמאופיינות בסימטריה רציפה. הגדלים הפיזיקליים הנגזרים ממחזורי גבול הם פרקטליים, אובייקטים המאופיינים בהיותם סימטריים תחת שינויי סקאלה בדידים.

בעבודה זו נתאר את פתרונות מרחב-הזמן של כבידת איינשטיין הקוונטית באמצעות ריצופים. לשם כך, אנו מציגים מיפוי בין משוואות חבורת הרנורמליזציה ובין תהליכי החלפה, שהינם תהליכים איטרטיביים שמייצרים מבנים מסובכים, כגון גבישים ופרקטלים. תהליכי החלפה מורכבים מחוק רקורסיה שמיוצג על ידי מטריצה. אנו משתמשים במיפוי שיצרנו על מנת לייצג זרימה של חבורת הרנורמליזציה באמצעות מטריצות ממימד 2x2, כאשר עם המטריצות שמצאנו נבצע תהליך החלפה על מנת ליצור ריצופים. את המיפוי אנו בונים לא בשימוש משוואות הזרימה של כבידת איינשטיין הקוונטית, אלא באמצעות דוגמאת עזר: תורת אפימוב.

תורת אפימוב מתארת את רמות האנרגיה של מערכת קוונטית לחלוטין. על מנת להבין אותה, אין צורך בידע קודם בתחום הכבידה הקוונטית. אך על אף שתורת אפימוב היא תחום רחוק מאוד מכבידת אינשטיין הקוונטית, תורות אלו חולקות מאפיין משמעותי, בו ניעזר כדי לשייך את שתיהן לאותה מחלקת שקילות - הגדלים הפרקטליים שלהן נגזרים מתוך פתרונות מחזורי גבול בזרימת חבורת הרנורמליזציה שלהן.

תורת אפימוב נולדה מתוך "אפקט אפימוב" ,שמתאר שלושה חלקיקים קוונטיים, חסרי ספין, שבין כל זוג קיימת אינטרקציה מושכת קצרת טווח. כאשר אורך הפיזור של מערכת

זו שואף לאינסוף ובו זמנית טווח האינטרקציה מתאפס, מופיע סט של מצבי אנרגיה קשורים עבור מערכת שלושת החלקיקים, על אף שאין מצבים קשורים עבור כל זוג בנפרד. סט מצבים קשורים אילו מהווה סדרה גאומטרית, שפקטור הגדילה שלה הוא מספר אוניברסלי, קרי שאינו תלוי בסוג האינטרקציה או במסות החלקיקים, למשל. המצבים הקשורים הללו יוצרים מבנה פרקטלי. את רמות האנרגיה של אפימוב מקבלים גם כאשר מופיע פתרון מחזור גבול בזרימת חבורת הרנורמליזציה של תורת אפימוב .

את המיפוי שאנו בונים ננסח תחילה עבור משוואות זרימת חבורת הרנורמליזציה של תורת אפימוב, שהינן משוואות פשוטות מאוד לעומת אלו של כבידת איינשטיין הקוונטית. באמצעות המיפוי שלנו נדגים כיצד רמות האנרגיה הפרקטליות של אפימוב מופיעות כריצוף מרחבי אותו נבנה על ידי תהליך החלפה שייצג את זרימת חבורת הרנורמליזציה. מן הדוגמה של תורת אפימוב נלמד על אופי המיפוי ועל הריצופים המתקבלים עבור פתרונות שונים לזרימת חבורת הרנורמליזציה ולאחר מכן, נשתמש בידע שרכשנו על מנת לבצע את אותו מיפוי על משוואות חבורת הרנורמליזציה של כבידת איינשטיין הקוונטית. עבור שתי התיאוריות שנבחנות בעובדה זו, אנו מוצאים את אותה התנהגות תחת המיפוי שלנו - נקודת שבת מתורגמת לריצוף מחזורי לחלוטין, ואילו מחזור גבול עובר מיפוי לריצוף פרקטלי. אנו מפרטים את התכונות שתהליכי ההחלפה הממופים מקיימים עבור סוגים שונים של פתרונות למשוואות הזרימה, ומוצאים שהמיפוי שלנו מתאים לכל זרימה ריבועית. המאפיינים המשותפים של תורת אפימוב וכבידת איינשטיין הקוונטית שאנו מוצאים מובילים אותנו לקבוע שהן משתייכות לאותה מחלקת שקילות תחת המיפוי שלנו.